Encoding Models of the Subcortical Whisker System

A thesis submitted to The University of Manchester for the degree of
Doctor of Philosophy in the Faculty of Life Sciences

2014

Kyle Davies

Contents

Word count: 27447

Abstract

The purpose of the brain is to allow animals to make rapid, complex responses to external circumstances, which requires sensitive and efficient sensory systems. The use that can be made of a sensory modality depends entirely on how the sensory information is encoded by the primary afferents; hence, understanding the early stages of a sensory pathway can help to understand how that sensory information can be used by the brain.

In this thesis we show that a simple Generalized Linear Model (GLM) describes stimulus response properties of the primary afferents of the rat whisker system to submillisecond precision, and analyse the parameters to reveal that the encoding mechanism of the system as a whole can be seen as a sparse, overcomplete basis of a low-dimensional projection of the stimulus space.

We also show that although the neurons of the Ventro-Posterior Medial (VPM) nucleus of the thalamus can be described well by a GLM, more powerful models, with nonlinear multi-feature stimulus dependencies, are able to predict their responses to a much greater degree of accuracy, and that therefore the form of the information entering the somatosensory cortex and the brain beyond has already undergone some degree of information processing.

Submitted by Kyle Davies for the degree of Doctor of Philosophy.

Entitled *Encoding models of the subcortical whisker pathway.*

Date of submission 3 June 2014.

No portion of the work referred to in this thesis has been submitted in support of an application for another degree or qualification of this or any other university or other institute of learning.

The author of this thesis (including any appendices and/or schedules to this thesis) owns certain copyright or related rights in it (the "Copyright") and s/he has given The University of Manchester certain rights to use such Copyright, including for administrative purposes.

Copies of this thesis, either in full or in extracts and whether in hard or electronic copy, may be made only in accordance with the Copyright, Designs and Patents Act 1988 (as amended) and regulations issued under it or, where appropriate, in accordance with licensing agreements which the University has from time to time. This page must form part of any such copies made.

The ownership of certain Copyright, patents, designs, trade marks and other intellectual property (the "Intellectual Property") and any reproductions of copyright works in the thesis, for example graphs and tables ("Reproductions"), which may be described in this thesis, may not be owned by the author and may be owned by third parties. Such Intellectual Property and Reproductions cannot and must not be made available for use without the prior written permission of the owner(s) of the relevant Intellectual Property and/or Reproductions.

Further information on the conditions under which disclosure, publication and commercialisation of this thesis, the Copyright and any Intellectual Property and/or Reproductions described in it may take place is available in the University IP Policy (see `http://documents.manchester.ac.uk/DocuInfo.aspx?DocID=487`), in any relevant Thesis restriction declarations deposited in the University Library, The University Library's regulations (see `http://www.manchester.ac.uk/library/aboutus/regulations`) and in The University's policy on Presentation of Theses.

Acknowledgements

I would like to thank my supervisors Rasmus Petersen and Marcelo Montemurro for their help and guidance for this thesis. I would also like to thank all of the members of the Petersen lab, in particular Michael Bale and Robin Ince for useful discussions as well as their work that has made this thesis possible.

For their endless support I'd like to thank my family, and for going through this with me I thank Jana Wendler.

Chapter 1

Introduction

The investigation of neural sensory coding can be traced through the entire history of neuroscience. Some early thought on the mechanisms of sensory representation can be found in the writings of Helmholtz and Müller, among others (Rieke et al., 1999). However, the experimental methods required to rigorously investigate the problem were not developed until later. The first work on individual sensory neurons, which laid the basis for the study of coding as it exists today, was that of Adrian (1926). In a series of experiments measuring electric potentials near nerve fibers, Adrian established that an individual sensory neuron either propagate signals along the length of its axon using stereotyped action potentials (or "spikes"), or it does not. This is the "all-or-nothing" principle that states that in vertebrates the communication of information to the central nervous system from a sensory neuron only occurs via the arrival of spikes. Since then the action of neurons, both peripheral and central, has been largely studied in terms of spikes, which can be measured extracellularly (Quian Quiroga and Panzeri, 2009).

Adrian used his data to propose the first hypothetical neural code: a "rate code", where stimulus strength is encoded by the number of action potentials recorded in a time window of approximately 300 ms after stimulus onset. However, there is no reason to believe this must be the only sensory code, and the possibility of codes using precise spike times has long been recognized (McCulloch and Pitts, 1943; MacKay, 1952). Between these two types of code is a necessary trade-off between robustness and information capacity: a rate code averages over a long time period, reducing the effect of noise in the number and timing of spikes, but each spike carries less

information than in a code using more precise timing information. It is still an open question to what extent the brain uses precise spike timing.

Advancements in technology and analysis techniques over the last few decades allow the study of neural coding characteristics in much greater detail. One useful model system that can be examined using these techniques is the rodent whisker system, which is the focus of this thesis.

1.1 Rat whisker system

The rodent whisker system is a useful model for the study of sensory coding and neural information processing, largely due to the readily apparent structural-functional organization at various levels of the neural pathway. This system is highly conserved across different rodent species, but here we will focus on the rat system in particular.

1.1.1 Whisker usage and texture discrimination

Rats, as nocturnal animals which frequently spend time in subterranean environments, often need to explore and investigate their surroundings without the benefit of light. One of the main ways they do this is with their whiskers, or vibrissae, which are arranged in a grid-like pattern on either side of their snout. Whiskers are identified by row and arc coordinates: rows are designated by the letters A to E and arcs by numbers, as shown in Figure 1.1A. In addition, there are a few whiskers not considered to be in any arc, designated α, β, γ, δ, also shown. In total, there are around thirty whiskers on each side of a rat's snout.

Rats use their whiskers by sweeping them back and forth across an object or surface of interest at around 10 Hz in an action known as "whisking". Sensing with whiskers is therefore generally an active process, though passive sensation of externally generated signals is also important (Kleinfeld et al., 2006; Diamond and Arabzadeh, 2013). Rats can use their whiskers to make remarkably fine discriminations, such as between a smooth surface and one machined with 50 µm deep grooves spaced 90 µm apart (Carvell and Simons, 1990, 1995), at a level of performance comparable with that of primates using their fingertips (Guić-Robles et al., 1989). Rats can also use their whiskers without whisking, for example when determining distances to objects (Diamond et al., 2008; Krupa et al., 2001).

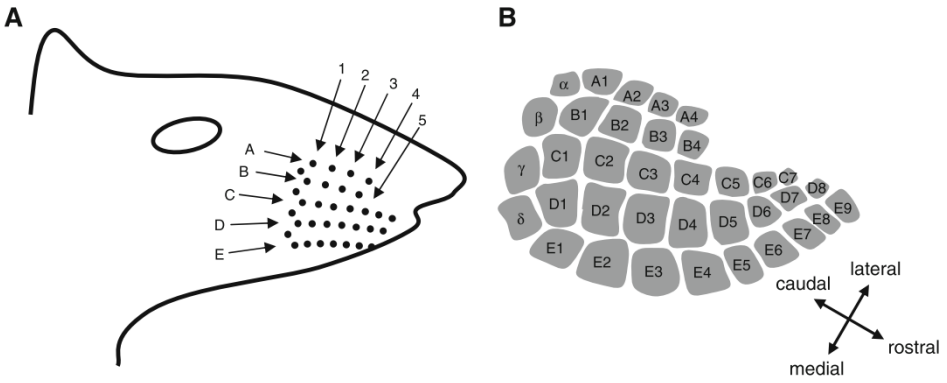

Figure 1.1: Topographic correspondence between whisker location on the snout and cortical barrels in rat. **A**, The location of whiskers on the snout, indicating rows A-E and arcs 1-5. **B**, The layout of cortical barrels as would be seen in a horizontal section through layer IV of the somatosensory cortex. There is a one-to-one correspondence between individual whiskers (also labelled are the barrels corresponding to whiskers α–δ, not considered to be in the arcs) and barrels, as seen in the layout, giving a strong indication that the neurons of the barrels process information from specific whiskers. From Petersen et al. (2009).

The precise mechanism of whisker texture discrimination is debated, with two main competing hypotheses. The first hypothesis follows from the observation that whiskers form resonant beams of different characteristic frequencies (Neimark et al., 2003). Textures have a signature of spatial frequencies in their deviations from an ideal plane. For example, a surface evenly spaced sinusoidal grooves could have a high spacial frequency (grooves close together), or a low one (grooves far apart). More complex textures can be thought of as quasi-periodic signals that have components of many spacial frequencies. These spacial frequency components can be translated by whiskers moving over the texture into a set of temporal frequencies, as whiskers of different lengths are optimally stimulated at their own resonant frequency. The set of whiskers that responds strongly to a certain texture contains an encoding of the various spatial frequencies of the texture (Neimark et al., 2003; Hartmann et al., 2003). The other main hypothesis is that textures are instead coded by temporal patterns of movement, called "kinetic signatures", that are induced in single whiskers (Arabzadeh et al., 2003, 2005; Hipp et al., 2006). Several different forms of the kinetic signature have been proposed, including various powers of mean whisker speed (Arabzadeh et al., 2003;

Gerdjikov and Bergner, 2010), the power spectrum of the whisker vibrations (Andermann et al., 2004), and other aspects of the form of whisker motion, particularly "slip-stick" events (Ritt and Andermann, 2008; Wolfe et al., 2008).

Rats are able to make reliable texture discriminations even when most of their whiskers have been clipped (von Heimendahl et al., 2007), though the integration of signals from multiple whiskers does improve discriminatory power (Lottem and Azouz, 2008; Krupa et al., 2001). This suggests that the spatial arrangement of stimulated whiskers is not necessarily important in texture coding (Diamond, 2010), counter to the resonance hypothesis, but consistent with the predictions of the kinetic signatures hypothesis. For texture discrimination at least, the encoding of kinetic features of single whisker dynamics seems to be sufficient.

1.1.2 Whisker system neuroanatomy

Vibrissal dynamics play an important sensory role for rats, so the information provided by whiskers must be translated into a useful representational signal in the brain. The discovery of the barrel cortex by Woolsey and Van der Loos (1970) was the first step to understanding the neural systems that perform this processing, and enabled the use of rodent whisker system as a model system for the study of sensory encoding (as well as broader neuroscientific research, such as plasticity and development, e.g. Feldman and Brecht (2005)).

The barrel cortex is a structure found in layer IV of the primary somatosensory cortex (SI), with distinguishable "barrels", separated by regions called "septa", that show a strong topographical correspondence to the layout of whiskers on the snout, as seen in Figure 1.1B. Since the barrel cortex was discovered, the anatomy of the neural pathways involved with whisker sensation has been laid out with increasing detail. Three primary afferent streams have been described, known as the "lemniscal", "extralemniscal", and "paralemniscal" pathways (Diamond et al., 2008; Alloway, 2008).

As shown in Figure 1.2, all three whisker neural pathway begin with the mechanoreceptors located in follicles at the base of whiskers (Rice and Munger, 1986). These receptors have a variety of morphologies and locations within the follicle (Rice and Munger, 1986), and their cell bodies are located in the trigeminal ganglion. The topographic organization found in the bar-

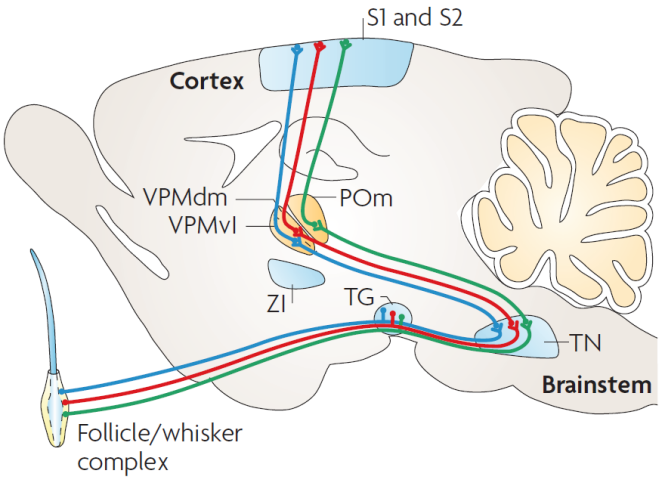

Figure 1.2: Schematic of the whisker sensory pathway. The cell bodies of the primary afferent neurons of all pathways of the system are located in the trigeminal ganglion. There is evidence that there is functional specialization already at the thalamic stage, with the paralemniscal pathway localized in the POm rather than the VPM. From Diamond et al. (2008)

rel cortex has not been shown for these neurons, though some studies have indicated that neurons innervating whisker rows A to E are located dorsally to ventrally, respectively (Leiser and Moxon, 2006). The possible relations between morphology and response have not been well explored (Diamond, 2010). Their response properties were initially investigated using "ramp-and-hold" stimulation protocols, in which whiskers are deflected to a constant angle before being released. The stimulus can be changed by varying either the magnitude of the whisker deflection or the speed with which it is displaced. These studies resulted in the classification of these primary afferents as rapidly adapting or slowly adapting (Zucker and Welker, 1969; Leiser and Moxon, 2007). Both types show a high transient firing rate in response to whisker deflection, but only slowly adapting cells show continued firing in response to a sustained deflection. Later studies have shown that when presented with more complex whisker stimuli, such as low-pass filtered white noise, they exhibit highly reproducible responses to repeated stimuli (Jones et al., 2004a), indicating the possibility for a highly informative spike-timing code.

Following the lemniscal pathway, the primary downstream neural structures are the "barrelettes" of the principal brainstem trigeminal nucleus

(Belford and Killackey, 1979). Axons from these cells project to "barreloids" in the dorso-medial region of the ventro-posterior medial nucleus of the thalamus (VPM) (Van Der Loos, 1976). The axons from the barreloids mainly terminate in the barrels of SI. Neurons in the barrelettes and barreloids are organized into highly structured anatomical maps, with identifiable clusters that have a one-to-one correspondence with individual whiskers, similarly to the barrel cortex. Although the barrels, barreloids and barrelettes respond most strongly to stimulation of a single "principal whisker", there is in fact considerable cross-whisker response, which has been measured using intracellular recordings in SI (Moore and Nelson, 1998) and thalamus (Brecht and Sakmann, 2002) and found to encompass most of the whisker pad at a sub-threshold level.

In the extralemniscal pathway, the mechanoreceptors also project to barrelettes, in the caudal region of the interpolar trigeminal nucleus. In turn, these project to the ventrolateral region of the VPM, corresponding to the "tails" of the barreloids. The pathway terminates in the septal regions of the barrel cortex, as well as in the secondary somatosensory cortex (Pierret et al., 2000). The septal regions show equal responsiveness to multiple whiskers, and seem to encode whisking dynamics (Alloway, 2008). As they also have projections to the motor cortex whisker representation, it may be the case that they are more strongly involved in regulation of whisker motor activity than the barrels (Alloway et al., 2004).

In contrast to the lemniscal and extralemniscal pathways, the paralemniscal pathway begins with neurons in the rostral region of the interpolar trigeminal nucleus that are not organized with spatial correspondence to the whiskers. They project primarily to the medial section of the posterior nucleus (POm) and the zona incerta (Pierret et al., 2000; Veinante et al., 2000). It is possible that the paralemniscal pathway integrates multiple-whisker information (Diamond et al., 1992; Ahissar et al., 2000).

At each successive stage in the main whisker pathway, there is a notable expansion in the number of neurons per whisker. It is estimated that each whisker follicle is innervated by around 150 mechanoreceptors (Lee and Woolsey, 1975; Rice et al., 1986), compared with approximately 250 neurons in each thalamic barreloid (Land and Simons, 1985) and around 10 000 per cortical barrel column (Welker and Van der Loos, 1986). A similar pattern has been noted in many other sensory pathways in different species, in-

cluding for example the cat visual system (Peters and Payne, 1993). These anatomical considerations show that the information processing context for neurons changes considerably at each stage, but it is not well understood why this expansion in the number of neurons exists. Coding studies have shown that a good reconstruction of a stimulus can be made using signals from, for example, the VPM or trigeminal ganglion (Jones et al., 2004a; Arabzadeh et al., 2006), so it may be hypothesized that this expansion exists to allow more sophisticated processing in the cortex. For example, it could allow useful adaptation to changing stimulus statistics, allow differential responses according to brain state, or enable integration of various aspects of the stimulus encoding, such as information from other whiskers. A good explanatory model of the neural code at each stage of the whisker pathway may be necessary in order to understand these kinds of anatomical features.

1.2 The neural coding problem

Understanding how sensory information from the external world is represented and transformed in the brain is an important aim of neuroscience. The process of turning stimuli into spike trains can be considered as a coding problem: what is the code that neurons use to represent the external world? However, neuronal responses are complex and variable, even when presented with repeated identical stimuli, which makes investigation of this code difficult. Unpredictable influences on neural activity include stochasticity in the biophysical mechanism of firing, changes in a neuron's activity such as variations in ion channel expression, and changes in brain state. We can study the earliest stages of sensory pathways, such as the neurons of the trigeminal ganglion, to minimize these sources of variability, but they are still present. Additionally we wish to understand the transformation of sensory representation through downstream areas of the brain, where such effects become more pronounced. Due to this variability, it is necessary to investigate the coding problem in the context of probability theory.

We consider a neuron's responses to be drawn from a distribution $P(r|x)$, where r is response and x the stimulus, that "translates" from stimulus to spike train. This distribution is sometimes called a "probabilistic dictionary" (Rieke et al., 1999), and represents all that we know about the

encoding mechanism used by a neuron. More accurately, it represents the coding activity of the measured neuron and all other stages between the applied stimulus and measured response, such as the primary afferents of the system. Determining an appropriate form for this dictionary is one of the major objectives of neural coding research.

Biologically, obtaining an accurate probabilistic dictionary means that we have a good idea of the computations that a neural pathway is performing. Focusing on sensory pathways allows us to study neural computations under conditions where the primary function of the system is essentially known and the input to the computations can be well controlled. Understanding the computations that take place at each level of the pathway may allow us to find commonalities that may generalize to information processing by neurons in general. Since the function of neurons is to process information, understanding neural activity on this somewhat abstracted level is a useful step towards understanding brain activity as a whole.

1.2.1 Quantifying the probabilistic dictionary

If infinite data were available, it would theoretically be possible to measure directly the probabilistic neural response to all stimuli. However, this is not practical and arguably not even useful for understanding the structure and function of neural responses. We therefore instead postulate a functional model and fit it to the data. This has the effect of reducing the very high (or infinite) dimension problem of estimating individual stimulus-response probabilities to a much lower dimension functional parameterization problem. Choosing an appropriate model is not a simple task, and requires balancing several objectives. First, the model should accurately reproduce at least the broadest aspects of neural behaviour in a predictive sense. A more detailed picture is better, but can conflict with the other objectives. Second, the model also must be theoretically and computationally tractable; if the model is too difficult to fit to data it cannot be used. Finally, the model should help to explain the action of neurons in a reasonably intuitive way; we wish to understand the neural code in terms of *what* information it is carrying (e.g. what features of whisker motion) and *how* it carries it (e.g. importance of precise spike timing). If this final objective is not met, it is difficult to say how the modelling has extended our understanding of the action of neural systems. Any deviations from the behaviour predicted by

the model can then be used as a starting point to investigate the influence of more complex interactions.

One widely used model is the Linear-Nonlinear Poisson (LNP) model (Marmarelis and Marmarelis, 1978; Chichilnisky, 2001), which takes the form[1]

$$\lambda_t = f\left(\mathbf{K}\vec{x_t}\right),$$

where λ_t is the rate parameter of a Poisson distribution determining the rate of spikes firing at time t:

$$P\left(r_t|x_t\right) = e^{-\lambda_t}\frac{\lambda_t^{r_t}}{r_t!}.$$

The "kernel" $\mathbf{K}$ is an m-by-n matrix (often with $m = 1$) that maps the n dimensional stimulus space to the m-dimensional "relevant subspace", where m may be far smaller than n. $\mathbf{K}$ can be interpreted as the neuron's receptive field, or stimulus features which modulate the neuron's response. In the whisker system, the stimulus $\vec{x_t}$ would describe the recent history of the whisker position. Each of the m rows of $\mathbf{K}$ would then be a linear feature of this stimulus, which could include velocity or acceleration, for example. The function f transforms the linear projection of $\vec{x_t}$ onto the kernel into a firing rate and serves to account for non-linearity in the neural response, such as saturation, thresholding, and positivity of firing rate. The LNP is useful as it is simple: the response depends only on a linear subspace of the stimulus at a certain time. It also is relatively easy to fit the model, only requiring estimation of $\mathbf{K}$ and f, as discussed in Section 1.2.2.

Although the LNP model has proved a useful context for investigating the coding problem, it is a very simplistic caricature of a real neuron. How well does it capture the important statistics of spike trains? Early neural response experiments had suggested that neural spike counts have a variance similar to their mean (Heggelund and Albus, 1978; Dean, 1981; Sestokas and Lehmkuhle, 1988; Shadlen and Newsome, 1998), as predicted by a Poisson model, but other studies, particularly of cells early in the sensory pathway, have found very low variability, even approaching the theoretical minimum for a count statistic (Miller and Mark, 1992; Berry and Meister, 1998; Kara et al., 2000; de Ruyter van Steveninck et al., 1997). Another obvious feature

[1] All vectors $\vec{v}$ in this thesis are column vectors unless explicitly transposed with the notation $\vec{v}^{\intercal}$. Matrices are represented by boldface capital letters: $\mathbf{A}$.

that is not accounted for by the LNP model is refractoriness: the model predicts the occurrence of small inter-spike intervals, potentially arbitrarily close to zero, while real inter-spike interval distributions display a lack of spikes within a refractory period.

The LNP model with a single-dimensional kernel is in fact a specific instance of a relatively broad model class known as Generalized Linear Models (GLM) (Nelder and Wedderburn, 1972; Paninski, 2004). The basic form of a GLM is given by the equation

$$\mathbb{E}\left[r_t\right] = g^{-1}\left(\vec{x_t}^\intercal \vec{k}\right).$$

Here, r_t is the neural response for the given stimulus $\vec{x_t}$, i.e. the number of spikes, $\vec{k}$ is the vector of model parameters, which are linear weights of the input components, and $g(.)$ is known as the "link function" describing the relationship between the linear projection of the stimulus and the expectation of the response. The distribution of the response variable can be taken to be any distribution in the exponential family, which includes for example the Poisson distribution and the binomial distribution.

It can be seen that the LNP model is a GLM by noting that for a Poisson distribution,

$$\mathbb{E}\left[r_t\right] = \lambda_t.$$

Then, g^{-1} corresponds to the tuning function f and $\vec{k}$ to a kernel $\mathbf{K}$ of one dimension. Noticing this relationship, it becomes easy to make the LNP more general, in order to overcome some of its weaknesses: we can simply allow more terms in the input $\vec{x_t}$, such as nonlinear functions of the stimulus, the spike history, and the spiking activity of other neurons.

1.2.2 Parameterizing neural models

Reverse correlation

The spike-triggered average (STA) and spike-triggered covariance (STC) methods have been the most widely used methods for investigating features that make a neuron fire, and are known together as reverse correlation methods.

The STA method is simple, intuitive, and widely-used (Ringach, 2004),

in which the feature estimate (the spike-triggered average) is given by

$$\hat{k}_{\mathrm{STA}} = \frac{1}{N} \sum_{t \in T} \vec{x_t},$$

where N is the number of spikes, T is the set of spike times, and $\vec{x_t}$ is the stimulus vector for the spike in time bin t, which for the whisker system would typically be a segment of the applied whisker position a length on the order of 100 ms. In other words the estimate for $\vec{k}$ is given by the average stimulus preceding a spike, or the mean of a sample from the spike-conditional stimulus probability distribution $P(\vec{x_t}|r_t = 1)$. Spike-triggered averaging has seen wide use in the field of neural coding, with some significant results and progress (Emerson et al., 1992; Sakai et al., 1995; Chichilnisky, 2001). One weakness of the method is that the STA only represents a single relevant dimension, so additional excitatory or inhibitory features to which the neuron is sensitive cannot be recovered.

The STC method is related to STA, but using the second order statistics (the covariance) of the stimulus leading up to a spike rather than only the mean. The neuron's receptive field is estimated using the covariance matrix of the stimulus vectors for the evoked spikes. Along some dimensions, the variance of the spike-triggering stimulus ensemble is similar to the variance of the non-spike-triggering ensemble, which suggests that these dimensions have no effect on the probability of the neuron firing. Along others, the variance may be smaller, indicating that when the stimulus is far from zero along that dimension there are few spikes; i.e. it is an inhibitory stimulus feature. The converse is true for dimensions of higher variance in the spike-triggering ensemble: they represent excitatory stimulus features.

An eigen-decomposition of the covariance matrix produces eigenvectors, which can be interpreted as stimulus features to which the neuron responds quadratically. The eigenvalues corresponding to the features indicate the relative importance of the feature in terms of how strongly a neuron responds to it: large eigenvalues indicate a dimension along which the variance is greater than that of the underlying stimulus, i.e. an excitatory feature and small eigenvalues indicate an inhibitory feature. The main improvements of the STC estimate over the STA is that it provides a relevant subspace of more than one dimension, and can reveal inhibitory as well as excitatory features. The STC method has been used in several studies in the whisker

coding literature, including Maravall et al. (2007) and Petersen et al. (2008).

However, it can be shown that in general STA and STC methods do not converge to the true relevant stimulus subspace, even if the LNP model is an accurate description of the neural response (Paninski, 2003). One obvious case of this for STA is if the tuning function f is symmetrical; the spike-triggered average will converge in the limit of infinite data to the zero vector in that case. This implies that the STA estimate will be spurious for any finite amount of data. Mathematically it can be shown that the STA is only guaranteed to converge on the true relevant subspace if the subspace is one dimensional, the stimulus distribution is radially symmetric, and the first moment of f is not zero. Deriving similar consistency constraints for the STC estimate shows that it will only converge if the stimulus is Gaussian distributed and the variance of the spike-triggering stimulus distribution projected onto the relevant subspace is sufficiently different from the total variance of the distribution (Paninski, 2003). Perhaps the most important of these constraints on the validity of reverse correlation methods is the requirement for a radially symmetric stimulus distribution. This constraint is immediately broken in the case of, for example, natural stimuli. Since the work of Rieke et al. (1995) and de Ruyter van Steveninck et al. (1997), which showed that sensory neurons in the bullfrog auditory system and fly visual system respectively had much more reliable responses to naturalistic stimuli, the use of natural stimuli has become increasingly prevalent in neural coding studies (e.g. Smyth et al. (2003); Talebi and Baker (2012)).

Additionally the STA and STC were developed to parameterize the LNP model, and do not have wider validity in different model classes. For example, models with recurrent connections between neurons, or those taking into account the effect of recent spiking history. If models to describe more complicated neural behaviour are required, more principled approaches must be taken to parameterizing them.

More sophisticated approaches

The STA and STC methods have been useful for investigating the receptive fields of neurons, but they have weaknesses as described above. A more general, widely studied, and highly successful framework is that of Bayesian inference (a thorough treatment of the foundations of the Bayesian approach can be found in many books; see, for example, Jaynes (2003) or MacKay

(2003)). In a Bayesian approach, as before, we postulate that the neural response can be characterized by a probability distribution described by a model, but to fit the model we describe our knowledge of the parameters using a probability distribution $p(\vec{k}|\mathbf{X}, \vec{r})$ (the "posterior" distribution). If our model provides an expression for the likelihood $p(\vec{r}|\mathbf{X}, \vec{k})$, as most common statistical models do, this leads automatically to expressions for the model parameters via Bayes' Theorem when combined with a prior $p(\vec{k})$:

$$p(\vec{k}|\mathbf{X}, \vec{r}) = \frac{p(\vec{r}|\mathbf{X}, \vec{k})p(\vec{k})}{p(\vec{r}|\mathbf{X})}$$

This approach brings several advantages, one of the most important of which for our purposes it can be applied to any model class for which a likelihood function is defined, including those for which reverse correlation estimates are invalid (artificial neural network models, for example). Another important aspect is the influence of the prior, which can be selected to encode some of the expectations we have regarding the form of stimulus dependence in the model, increasing the parameters' interpretability and reducing the amount of data required for accurate estimation (Park and Pillow, 2011).

Despite the theoretical simplicity of Bayesian inference, practical issues remain, the most important of which being computational tractability. In general there is not an analytic expression for the posterior distribution and approximations must be made. The specific solutions to these issues and other subtleties are discussed in the methods sections of chapters 2, 3, and 4.

1.3 Aims

Although many aspects of neural coding in the whisker system and in sensory systems in general are reasonably well understood, there are still important unanswered questions. As discussed above, in order to investigate these problems in a rigorous way, it is necessary to have a good quantitative model of the response.

The overarching aim of the study is to understand the sensory code in the early stages of the rat whisker pathway using a statistical modelling approach, and identify effective modelling methods for the neural coding problem. This is primarily achieved by testing how well the models predict

neural responses and investigating any areas where the models do not work well. This is particularly important in the context of the most biologically relevant stimuli, in this case naturalistic textures.

1.3.1 Understanding the input into the whisker sensory pathway

Studies have been done into the earliest stage of the whisker pathway, the trigeminal ganglion, on a qualitative level (Zucker and Welker, 1969; Lichtenstein et al., 1990) and on a more mechanistic—though still empirical—level (Mitchinson et al., 2004; Leiser and Moxon, 2007), but we wish to understand the information carried by the sensory pathway at the initial stages from a coding perspective. If a good, predictive model of the responses of trigeminal ganglion neurons can be found, then we can say with a reasonable degree of certainty that we have some understanding of the information entering the sensory system.

1.3.2 Investigating the transformation in the neural code in the early stages of the pathway

Following the sensory pathway from whisker to cortex, at each stage the anatomical conditions change. Is this associated with a change in coding mechanisms? Studies such as Bale and Petersen (2009) suggest that it is, but we wish to confirm and explore this more rigorously, applying statistical modelling techniques to the responses found in the VPM thalamus.

1.3.3 Investigating the neural code with respect to naturalistic stimuli

Most work on whisker somatosensory coding to date has used somewhat unnatural stimuli such as ramp-and-hold or sinusoidal stimuli. However, in order to understand a neural code it is important to investigate it under rich stimulus conditions, ideally similar to those encountered in normal behaviour. This can be justified from an evolutionary perspective: the neural code would have been honed over the evolutionary history of rodents to best represent and discriminate the kinds of stimuli important to rodent survival. We therefore make use of dynamic whisker stimuli, including naturalistic stimuli.

The use of natural stimuli in the whisker system is difficult as it typically requires chronic recordings from awake animals, which means experimental control of the stimuli is limited. To make recordings from strongly controlled repeated trials it is useful to use "naturalistic" stimuli, stimulus patterns measured from real whisker movements. Such naturalistic stimuli are beginning to become available thanks to high-speed video cameras (Wolfe et al., 2008), and are used in the experiments that provided the data for this study, described in detail in Chapter 2.

An important aim of the analysis is therefore to investigate sensory coding in the context of naturalistic stimuli. An important check on the models is how well they predict the measured responses to these stimuli.

1.4 Author contribution

The research presented in this thesis was highly multi-disciplinary and as such represents the work of multiple individuals. In particular, the research leader Rasmus Petersen oversaw much of the research direction, experimental design, and data analysis.

Most experimental work was carried out by Michael Bale, who also was heavily involved in the experimental design. Greta Santagata and Oliver Freeman assisted with experimental work, and Robin Ince set up some of the initial data handling software.

The author's contribution consisted of the computational and statistical modelling aspects of the work. This involved data handling, model selection, implementation, fitting, evaluation, and refinement. All computational work was performed using software custom written using MATLAB R2011a (The Mathworks, Inc., Natick, Massachusetts, United States).

1.4.1 Publications and presentations resulting from this work

Bale, M. R., Davies, K., Freeman, O. J., Ince, R. A. A., & Petersen, R. S. (2013). Low-Dimensional Sensory Feature Representation by Trigeminal Primary Afferents. *Journal of Neuroscience*, 33(29), 1200312012.

Davies, K., Bale, M. R., Petersen, R. S. Bayesian model-based investigation of sensory coding in rat trigeminal ganglion. University of Manchester Faculty of Life Sciences Research Symposium. The Armitage Centre, Manchester UK. 21 September 2012.

Davies, K., Bale, M. R., Freeman, O. J., Petersen, R. S. Predicting the response of neurons to naturalistic whisker motion with submillisecond precision. BNA Festival of Neuroscience. The Barbican Centre, London UK. 8 April 2013.

Davies, K. Sensory coding by collective neuronal action in the thalamus. Lecture. Systems Biology Inter-DTC Conference. Manchester Interdisciplinary Biocentre, Manchester UK. 22 June 2011

Davies, K. Sensory coding in the trigeminal ganglion. Postgraduate prize lecture. University of Manchester Faculty of Life Sciences Research Symposium. Sugden Centre, Manchester UK. 19 September 2014.

Chapter 2

A generalized linear model of trigeminal ganglion neurons reveals population representation of whisker motion

2.1 Introduction

The primary afferent neurons of any sensory modality determine what information is available to downstream neurons for further processing and use. Understanding the transduction properties of a sensory system is therefore key for understanding wider action of the system. The primary afferents in the rodent whisker system are mechanoreceptors that innervate the whisker follicle, whose cell bodies are located in the trigeminal ganglion (Rice et al., 1986; Ebara et al., 2002). Forces on an animal's whiskers induce strains in the follicles, deforming the mechanoreceptors and causing them to fire action potentials. The firing rate of these neurons has been shown to be modulated reliably by a number of features of both passive and active whisker deflection, including position, velocity, and direction (Zucker and Welker, 1969; Gibson and Welker, 1983; Lichtenstein et al., 1990; Jones et al., 2004a).

Previous studies have revealed that these neurons have highly reliable

responses and extremely precise spike-timing when stimulated by complex whisker motion such as white noise Jones et al. (2004b). Attempts have been made to describe these properties using bio-mechanically motivated models of the whisker follicle (Mitchinson et al., 2008; Lottem and Azouz, 2011). However, these methods have required hand-tuning of the model parameters and the resulting models do not have a simple interpretation in terms of the information encoded by the spikes. Here we take a different approach, using the GLM framework to investigate the response properties of the primary afferents to dynamic whisker stimulation. This approach has several advantages, one of the most important of which is that the log posterior probability distribution of the parameters is convex (Paninski et al., 2007). This makes it computationally tractable to automatically fit the model parameters using a Bayesian approach, and summarize the posterior accurately. The parameters can then be interpreted in an intuitive way, in terms of stimulus filtering and the information encoded in the pattern of action potentials.

The majority of the work contained in this chapter was published in Bale et al. (2013).

2.2 Methods

2.2.1 Electrophysiology

Recordings (performed by M. Bale) were taken from anaesthetized adult Wistar rats ($n = 8$, mean weight 193 g, SD 24 g, urethane anaesthetic at $1.5\,\mathrm{g/kg_{body\ weight}}$) that were placed in a stereotaxic apparatus. The body temperature of the rats was maintained at 37.5 °C. A piezoelectric motor was used to insert a tungsten microelectrode (8 MΩ to 10 MΩ) into the trigeminal ganglion. Extracellular recordings were amplified, sampled at 24.4 kHz and bandpass filtered (300 Hz to 3000 Hz) before being spike-sorted to obtain spike trains from individual units (see Section 2.2.3).

2.2.2 Whisker manipulation

The spiking activity of individual neurons was measured in response to deflection of their innervated whiskers. All whiskers were trimmed to a length of 5 mm and manually stimulated until a clearly responding unit was identified in the measured electrophysiological signal. Once a clearly responding

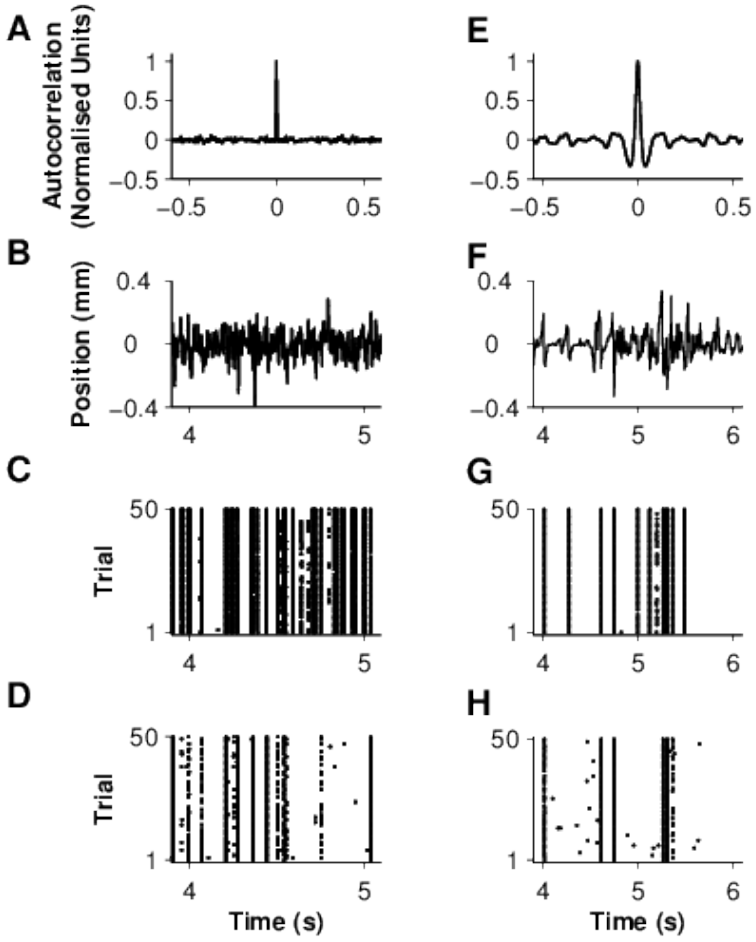

Figure 2.1: Samples of the whisker stimuli and responses. **A**, Autocorrelation of the white noise stimulus. **B**, Snippet from the white noise stimulus, showing whisker position against time. **C, D**, raster plots for two example units for white noise. Each point is a spike plotted by its trial number and when it occurred relative to the stimulus. **E**, Autocorrelation of the texture stimulus. **F**, Snippet from the texture stimulus. **G, H**, raster plots for the same units as **C** and **D** for texture.

unit was found, its innervated whisker was inserted into a piezoelectric stimulator capable of applying a rostro-caudal displacement of ±0.8 mm to the whisker relative to its resting position, to deflect the whisker according to the stimulus protocol.

The stimulus protocol consisted of two different types of stimulus, hereafter called the "white noise" and "naturalistic" stimuli. The white noise stimulus was created by sampling pseudorandom white noise with a Gaussian amplitude distribution at 12.2 kHz, before convolving with a Gaussian kernel with a standard deviation of 1.6 ms. This was done in order to restrict the stimulus power in frequencies at and above the resonant frequency of the piezoelectric stimulator, improving the fidelity of the induced whisker motion. The autocorrelation structure of the resulting stimulus is shown in Figure 2.1A, and a 1 s sample of the stimulus is shown in Figure 2.1B.

The naturalistic stimulus was created from optical recordings of whisker motion in the rostro-caudal direction captured by Wolfe et al. (2008). A linear CCD array was used to record whisker position while awake animals were palpating a textured surface (grade P150 sandpaper). Segments of the whisker position recorded during contact with the surface were joined together to form a 10 s sequence. The autocorrelation structure and a 2 s sample of this stimulus are shown in Figure 2.1C and D respectively.

The whisker manipulation protocol consisted of 50 epochs, each of which contained three 10 s sequences: the naturalistic sequence, a repeated white noise sequence, and a non-repeated white noise sequence that was unique to each epoch. The response to the 500 s non-repeated the white noise stimulus was used to fit the model parameters, while the quality of the model description was tested by comparing its predicted response to the repeated white noise and naturalistic stimuli with the experimentally measured response.

2.2.3 Spike sorting

Spike trains from individual units were obtained from the extracellular recordings using a standard spike-sorting approach: first, 2 ms windows of the recorded potential were extracted whenever the potential crossed a threshold. The dimensionality of these windows was reduced using principal component analysis to 5, and clusters discovered by the expectation-maximization fit of a Gaussian mixture model. For this dataset, only one spike train was ever obtained from each recording made. Units that did not

exhibit a clear refractory period were discarded. A total of 32 neurons were recorded.

2.2.4 Jitter estimation

A measure of the trial-to-trial variability in spike timing, known as "jitter", was calculated for each neuron using the method described by Montemurro et al. (2007). First, firing events were found by binning responses to a stimulus at 1 ms precision and taking each bin in which the firing rate was at least 50 % of the units maximal firing rate. The relative timing of spikes within ±2 ms of these events were pooled and the jitter was calculated as the standard deviation of these time differences.

2.2.5 Generalized linear model

To investigate the coding properties of trigeminal ganglion neurons, we fitted GLMs to single unit responses to the non-repeated white noise (Nelder and Wedderburn, 1972; Truccolo et al., 2005; Paninski, 2004; Paninski et al., 2007). To perform this analysis, the observed spike trains were discretized into bins (time bin widths in the range 0.125 ms to 10 ms, hereafter denoted by the variable τ) and represented by the vector $\vec{r}$: element r_t was 1 if one or more spikes occurred in time bin t, and 0 otherwise. The whisker stimulus was represented as a matrix, $\mathbf{X}$, with rows denoted $\vec{x_t}^\intercal$. The elements of these rows were samples of the applied whisker position in the interval −30 ms to 10 ms relative to the time bin t, sampled at 1 ms intervals (so the matrix $\mathbf{X}$ had 41 columns). This resampling was performed in order to reduce the number of model parameters while maintaining essentially all of the stimulus information: the original sampling rate was 12.2 kHz, but the stimulus had an autocorrelation time of 1.6 ms, negating the need for so many samples. Note that this choice of stimulus representation is independent from the time bin width.

GLMs provide a natural way to account for, and estimate, both the receptive field of a neuron and spike-history effects such as refractoriness. The input to the GLM consisted of both the stimulus time series and the recent spiking history of the neuron. These inputs were linearly filtered, and passed through a nonlinear function. A probabilistic (Bernoulli) spike generator used the resulting output to produce a sequence of ones and zeros

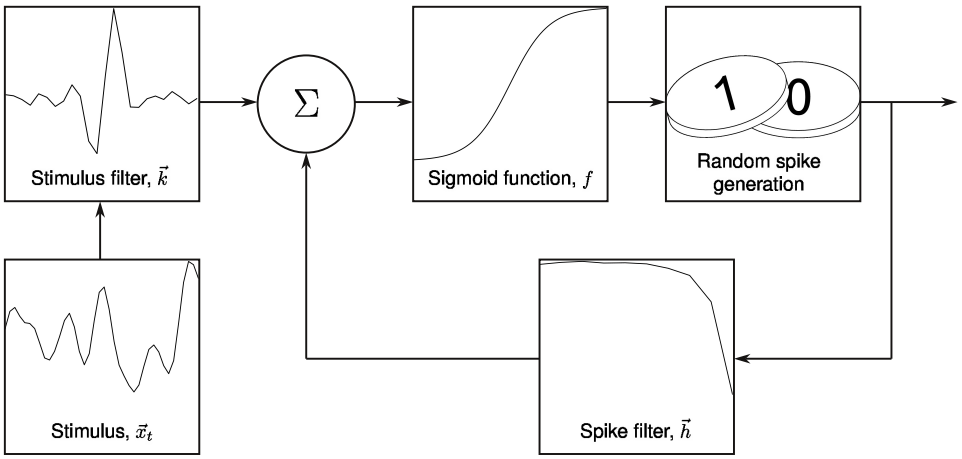

Figure 2.2: Generalized Linear Model schematic. The projection of the recent whisker stimulus $\vec{x_t}$ onto the stimulus filter $\vec{k}$ (i.e. $\vec{k}^\intercal \vec{x_t}$ is summed with the contribution from the spike history (projection of $\vec{n_t}$ onto the spike history filter $\vec{h}$) and the constant term b. The result is passed through the nonlinear function $f(.)$ to obtain the probability of a spike in the time bin t.

representing the presence or absence of spikes. A schematic of the model is shown in Figure 2.2. The functional form of the model that we used was as follows:

$$p\left(r_t = 1 | \vec{k}, \vec{h}, b, \vec{x_t}\right) = \pi_t = f\left(\vec{k}^\intercal \vec{x_t} + \vec{h}^\intercal \vec{n_t} + b\right). \tag{2.1}$$

The probability of firing in the model depended on three terms. The first term was the scalar product between the whisker stimulus vector $\vec{x_t}$, and the "stimulus filter" $\vec{k}$, which determined the kinetic features of whisker motion to which the model neuron was sensitive. The second term was the scalar product between the recent spiking history (referred to as the "spike feedback" term), represented by $\vec{n_t}$, and the "spike history filter" $\vec{h}$. $\vec{n_t}$ consisted of 10 elements $n_{t;1}, n_{t;2}, \ldots, n_{t;10}$ and was defined in terms of Gaussian basis functions, where the basis functions had width $\sigma = \frac{1\text{ms}}{\tau}$ (i.e. equal to 1 ms in units of the time bin width) and centres $\mu_j = \tau(t - (2j-1)\sigma)$. If these are collected into a basis change matrix $\mathbf{B}$ where $\mathbf{B}_{ij} = \exp -\frac{(\mu_j - \mu_i)^2}{2\sigma^2}$, the expression for $\vec{n_t}$ is then

$$\vec{n_t} = \mathbf{B}\overrightarrow{r_{t-m:t}}$$

where $m = \text{ceil}\left(\frac{20\text{ms}}{\tau}\right)$ and was the number of previous time bins taken into account. Therefore for any value of the time bin width, 20 ms of the spiking history was represented by the 10 values of $\vec{n_t}$. As an example, for time bins with a width of 2 ms, the Gaussian basis functions are centered exactly on the previous time bins. Depending on the form of $\vec{h}$, the probability that the model fired a spike could be suppressed by recent spiking (refractoriness) and/or facilitated (burstiness). The final term of Equation 2.2 was the constant input b, which set the spontaneous firing rate of the model. The nonlinear function $f(.)$ was the logistic function $f(x) = \frac{1}{1+\exp(x)}$

The expression for the probability π_t of finding a spike in a time bin t, as given in Equation 2.1, was used with the Bernoulli distribution to calculate the full log-likelihood:

$$\log p(\vec{r}\,|\,\vec{k}, \vec{h}, b, X) = \sum_t r_t \pi_t + (1 - r_t)(1 - \pi_t) \tag{2.2}$$

We used an uncorrelated Gaussian prior for the parameters, with the scale determined by hyperparameters α and β:

$$\log p\left(\vec{k}, \vec{h}\,|\alpha, \beta\right) = \frac{\alpha}{2}\left\|\vec{k}\right\|_2^2 + \frac{\beta}{2}\left\|\vec{h}\right\|_2^2. \tag{2.3}$$

Here, $\|.\|_2^2$ represents the squared 2-norm, i.e. $\|\vec{x}\|_2^2 = \sum_i x_i^2$. The parameter b had a flat prior (i.e. it was fitted by maximum likelihood).

The GLM was fitted by finding the parameters b, $\vec{k}$, and $\vec{h}$, which maximized the probability of the model given the data (the spike train $\vec{r}$ and the stimulus matrix $\mathbf{X}$), known as the Maximum *A Posteriori* (MAP) fit. The full log-posterior $\log p(\vec{k}, \vec{h}, b|\vec{r}\mathbf{X})$ is given by the addition of Equations 2.2 and 2.3 along with a constant that does not affect the MAP parameters.

GLMs possess the convenient property that the log-posterior probability is a concave function of the parameters, and therefore has a single, global maximum (Paninski et al., 2007). This means that the MAP parameters can easily be located by the iteratively reweighted least squares method (Nelder and Wedderburn, 1972), equivalently known as the Newton-Raphson method.

A type-II maximum likelihood procedure was used to fit the hyperparameters that determined the scale of the filters $\vec{k}$ and $\vec{h}$ (MacKay, 1992; Park and Pillow, 2011). This is an iterative procedure that alternates be-

tween finding the MAP fit for the current hyperparameters and updating the hyperparameters to maximize the marginal likelihood. The marginal likelihood $p\left(\vec{r}|\mathbf{X}\right)$ was calculated using the Laplace approximation for the posterior. In this approximation, the posterior distribution is represented by a Gaussian with mean given by the MAP parameters and covariance given by the inverse of the Hessian matrix of the log-posterior evaluated at this point. The marginal likelihood was then maximized by updating the hyperparameters according to the fixed-point formulae:

$$\alpha_{\text{new}} = \frac{d_k - \alpha \text{Tr}(\mathbf{C}_k)}{\left\|\vec{k}\right\|_2^2},$$

$$\beta_{\text{new}} = \frac{d_h - \beta \text{Tr}(\mathbf{C}_h)}{\left\|\vec{h}\right\|_2^2}.$$

Here, d_k and d_h were the dimensionality (number of parameters) of $\vec{k}$ and $\vec{h}$ respectively. $\mathbf{C}_k$ and $\mathbf{C}_h$ are the posterior covariance submatrices corresponding to the parameters in $\vec{k}$ and $\vec{h}$. This procedure was iterated 5 times.

2.2.6 Model evaluation

Once the best-fitting GLM parameters had been identified for a given unit and time bin duration, the next step was to assess the predictive power of the model. To do this, we used the neural responses evoked by the repeated stimulus sequences (50 each of white noise and texture) to measure the "experimental" peristimulus time histogram (PSTH). Then, we used the repeated stimulus sequence as input to the model and obtained its predicted response. By repeating this 50 times and averaging the responses, we obtained the "predicted" PSTH. To compare the quality of the prediction, the Pearson correlation coefficient between the experimental PSTH and predicted PSTH was calculated for each unit.

This correlation coefficient was corrected for sampling error as described by Sahani and Linden (2003). Briefly, we attempt to eliminate the unpredictable element from the response variance (over time) by using the estimator

$$\text{Var}\left[\vec{r}\right] = \frac{1}{N-1}\left(N\text{Var}\left[\langle\vec{r}\rangle\right] - \langle\text{Var}\left[\vec{r}\right]\rangle\right) \tag{2.4}$$

instead of the plain $\mathrm{Var}\left[\langle\vec{r}\rangle\right]$. Here $\langle.\rangle$ denotes the average over trials and N is the number of elements in $\vec{r}$.

This correction accounts for the fact that there may be be an unpredictable element in the measured spike trains. That is, in a trial indexed by i, $\vec{r}^{(i)} = \vec{\mu} + \vec{\eta}^{(i)}$ where $\vec{\mu}$ is the stimulus-dependent component common over trials and $\vec{\eta}^{(i)}$ is a zero-mean noise component that varies over trials. The expression given in 2.4 can be shown to cancel (in expectation) the variance in the signal due to the noise in the calculation of the correlation coefficient.

2.2.7 Response delay estimation

An estimate of lag between the stimulus feature the model was responsive to and the spike time was calculated for each cell. This was calculated as a weighted average:

$$T = \frac{\sum_i k_i \Delta t_i}{\sum_i k_i},$$

which could be thought of as the "centre of mass" of the filter $\vec{k}$. Δt_i is the time of each component of k_i relative to the spike time, i.e. $-30\,\mathrm{ms}$ to $10\,\mathrm{ms}$ in $1\,\mathrm{ms}$ intervals, as the stimulus was sampled at $1\,\mathrm{ms}$.

2.2.8 Feature space analysis

We characterized feature selectivity by applying a Principal Component Analysis (PCA) to the set of stimulus filter vectors. PCA can be thought of as finding a new orthonormal set of basis vectors for a vector space that is ranked by the variance of the data in the direction of each basis vector. As an example, if all of the stimulus filters were exactly the same shape (for example, a velocity filter) and differed only in scale, PCA would recover that one feature and show that it accounted for all of the variance in the data. For real data, not all the variance will be in one dimension, but it may be that only a few dimensions account for most of the difference in shape between the stimulus filters.

Formally, PCA is performed by applying the eigendecomposition to the covariance matrix of the filters $\mathbf{K}^\intercal\mathbf{K}$, where the rows of $\mathbf{K}$ are the stimulus filters for all of the models. This decomposition yields eigenvectors (the principal components), and corresponding eigenvalues that are equal to the

variance of the set of filters along the component. We defined the relevant feature space as the hyperplane spanned by the principal components accounting for 95 % of the variance in the set of stimulus filters.

2.3 Results

The aim of this study was to determine whether the response characteristics of trigeminal ganglion neurons could be adequately determined by a simple, easily-fitted model, and if so what could be determined about the sensory code employed by these neurons. We begin by describing some of the general response properties of the neurons to applied whisker motion.

2.3.1 Response of trigeminal ganglion neurons to whisker motion

The general properties of the response of the primary afferents to applied whisker motion were consistent with previous work on this stage of the whisker pathway: the neurons responded reliably, with high temporal precision (Jones et al., 2004a; Arabzadeh et al., 2005; Lottem and Azouz, 2011).

The recorded units displayed very low spontaneous firing activity (median across units $0.04\,\mathrm{spike\,s^{-1}}$, IQR $0\,\mathrm{spike\,s^{-1}}$ and $0.14\,\mathrm{spike\,s^{-1}}$). Applied whisker motion evoked robust spiking patterns, for both white noise and texture stimuli. As shown in Figure 2.3C, D, G, H, the form of the response was typically highly reproducible and temporally precise single-spike events. This is illustrated by the vertical structure in these figure panels; they show times where there was some feature in the stimulus that evoked an action potential from the recorded neuron on nearly every trial. These are interspersed with periods of virtually no spiking activity, with very little noise in the form of spikes on individual trials. Significantly higher firing rates were evoked by white noise stimuli (median $12.0\,\mathrm{spike\,s^{-1}}$ for white noise against $2.3\,\mathrm{spike\,s^{-1}}$ for texture $p = 7 \times 10^{-7}$, Wilcoxon rank-sum test). Across the recorded population there was a wide spread in the evoked firing rates (IQR $4.1\,\mathrm{spike\,s^{-1}}$ to $43.2\,\mathrm{spike\,s^{-1}}$ for white noise, $0.9\,\mathrm{spike\,s^{-1}}$ to $3.9\,\mathrm{spike\,s^{-1}}$ for texture).

A measure of the temporal precision ("jitter") of the neurons was obtained by calculating the standard deviation of spike times in 4 ms windows centered on well-defined firing events as described in Section 2.2.4. The cal-

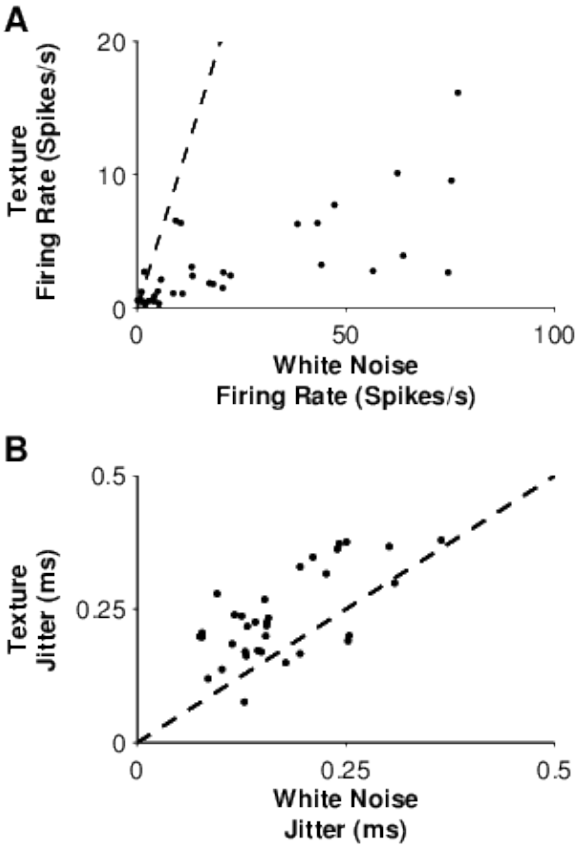

Figure 2.3: Basic properties of the responses of the trigeminal ganglion neurons. **A**, each point shows the firing rate of a neuron under texture stimulation against firing rate under white noise stimulation. **B**, the analogous plot for the jitter of each neuron. Dashed lines in both panels denote equality.

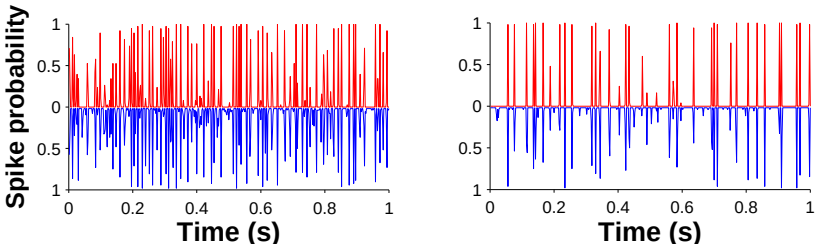

Figure 2.4: Experimentally measured PSTH evoked by white noise compared with the GLM-predicted PSTH for two example cells at a time resolution of 1 ms. The measured PSTH is plotted above the y-axis in red, with the predicted one below in blue. The y value for each time bin is the proportion of trials in which the bin contained a spike.

culated jitters can be seen in Figure 2.3B. The median jitter in response to white noise was 0.15 ms (IQR 0.13 ms to 0.23 ms), while for texture it was slightly higher at 0.22 ms (IQR 0.13 ms to 0.23 ms). Every unit had a jitter below 0.5 ms. The fact that this is below the stimulus correlation time (1.6 ms), indicates that a pure kinetic feature model of the response is inadequate, as it would not be capable of accounting for such temporally precise response charaacteristics.

2.3.2 Predictive power of the GLM

First, we asked whether this model class is capable of predicting the response of the primary afferents to stimuli different from those used in the fitting procedure, and therefore whether it forms an appropriate description of the encoding properties of these neurons. Figure 2.4 shows that the predicted response to a white noise stimulus typically showed a very good correspondence with the experimentally measured PSTH, matching both the timing and amplitude of spiking events. In order to quantify the quality of this correspondence, we calculated a modified Pearson correlation coefficient between the predicted and experimental PSTHs for each measured unit (see Section 2.2.6). The neurons shown in Figure 2.4 were representative of the population, with prediction coefficients of 0.95 and 0.93 respectively. The median prediction coefficient across the population was 0.92 (IQR 0.90 to 0.94). This showed that the GLM was capable of capturing the response of the neurons to white noise stimuli very well.

We wished to see whether the GLMs that had been fitted on white noise

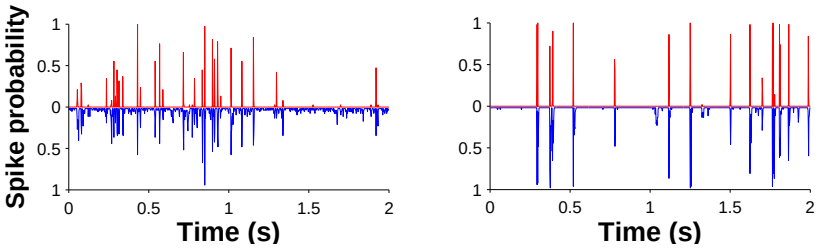

Figure 2.5: Experimentally measured PSTH evoked by naturalistic stimulus compared with the GLM-predicted PSTH for two example cells at a time resolution of 1 ms. The measured PSTH is plotted above the y-axis in red, with the predicted one below in blue. The y value for each time bin is the proportion of trials in which the bin contained a spike.

data could also predict the response of the neurons to more naturalistic whisker stimulation. This is not a trivial issue, as good generalization from white noise data is not guaranteed (Talebi and Baker, 2012). Although white noise explores the stimulus space in a comprehensive and unbiased way, it may be that a neuron exhibits complex response characteristics only in the presence of rich features such as those found in natural stimuli. This important region of stimulus space may be under-sampled when using white noise, leading to poor generalization even with an appropriate model.

We therefore carried out the same analysis with the repeated naturalistic stimulus. Shown in Figure 2.5 is a comparison between the measured PSTH and predicted response for the same example cells as before. Again the model output predicts both the timing and amplitude of the spiking events well: the models for these two neurons had prediction coefficients of 0.78 and 0.85. These were again typical of the population, which had a median prediction coefficient of 0.86 (IQR 0.71 to 0.89).

The prediction quality results are fully summarized in Figure 2.6. The histogram at the bottom of the figure shows that a majority of model predictions had a prediction quality coefficient in the range 0.9 to 1 for the white noise stimulus, with only two units falling below the 0.8 mark. Panel A shows shows that while the prediction quality coefficients for the texture stimulus were universally lower than those for white noise they were typically close to the white noise value. The histogram on the left of panel A shows that again a majority of coefficients were above 0.8, though more were below that level than for white noise, and one was as low as 0.3.

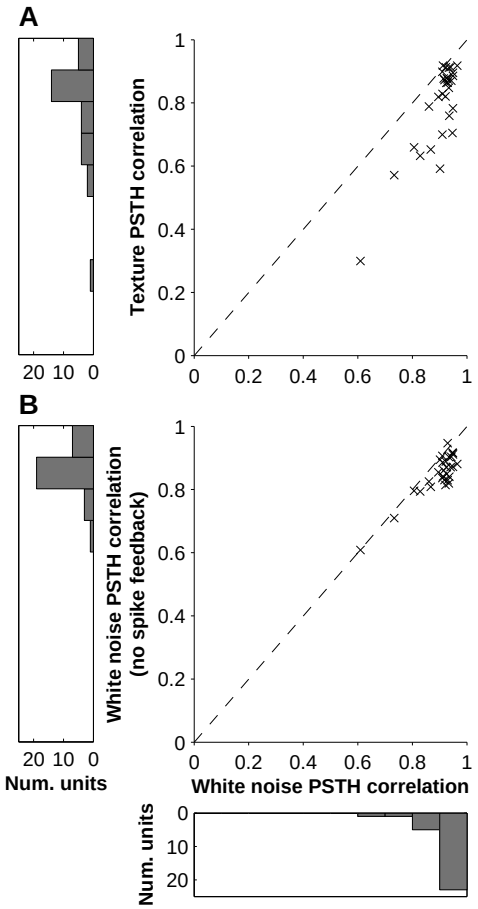

Figure 2.6: Summary of the prediction coefficients across the population of recorded cells at 1 ms time resolution. **A**, Scatter plot of the prediction quality coefficient for the white noise stimulus against that for texture. **B**, Scatter plot of the prediction quality coefficient for the white noise stimulus with the spike feedback term against that without the spike feedback. The histograms show the quantity of units with prediction quality coefficients in bins with edges [0.0, 0.1, ..., 0.9, 1.0].

The PSTH representation of the response of a neuron to a stimulus captures important aspects of the response, but loses other information such as inter-spike correlations. As a further check for the model, we checked its predictions against another feature of the response: the relationship between the variance and mean of the spike count across trials. The primary afferents of the whisker system were so reliable in their response to the stimuli

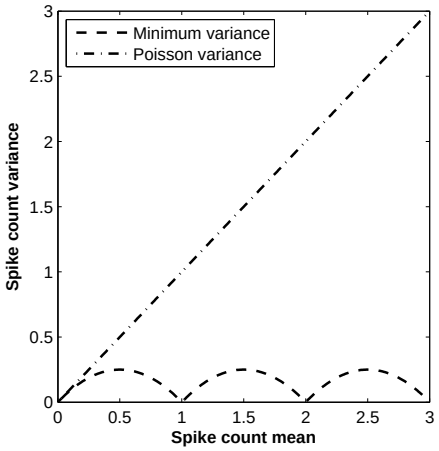

Figure 2.7: Theoretical spike count variance versus mean plots for the minimum possible variance (equal to $f(1-f)$ as described in the text), and a Poisson distribution (equal to the mean).

under these experimental conditions that the variance in their spike counts in longer time bins (20 ms) came close to its theoretical minimum as a function of the mean spike count (de Ruyter van Steveninck et al., 1997). The minimum arises from the fact that an increased mean spike count can be due either to extra spikes occurring within trials or across trials. For example, with two trials, a mean spike count of 1 could be either from both trials having a single spike or one trial with two spikes and the other with zero. In the first case the variance is zero, while in the second it is 1. In general, the minimum possible variance is given by $\sigma^2 = f(1-f)$, where f is the fractional spike count mean (i.e. count mean $-$ floor(count mean)), which occurs when all trials have spike counts of either n or $n+1$. Plotting the variance against the mean reveals the characteristic "scalloped" shape of this minimum, as shown in the theoretical case in Figure 2.7, and for two example cells in Figure 2.8 A1 and A2. This is in contrast to a Poissonian firing pattern, in which the variance of the spike count is equal to the mean. A close match was seen between the experimental data and the equivalent plot for the model's predicted response for these cells (Figure 2.8 B1 and B2), indicating that the model captures enough of the behaviour of the neurons to recreate aspects of the response, such as spike train autocorrelation, beyond the simple firing rate.

We summarized this behaviour across the population using the Fano

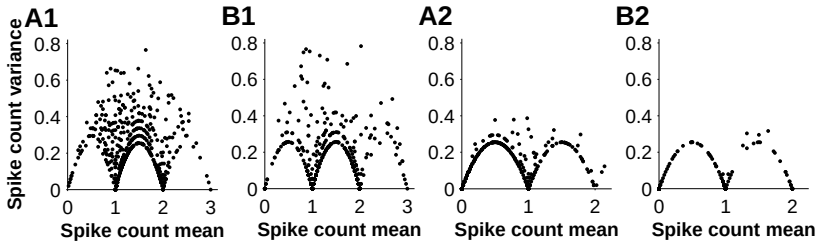

Figure 2.8: Variance of spike count across trials in 20 ms bins plotted against spike count mean across trials, for two example cells. **A1** and **A2**, Results calculated from experimental data. **B1** and **B2**, The corresponding results from GLM predictions.

factor, the mean over time bins of the spike count variance over the spike count mean. This is shown for both the white noise and texture stimuli in Figure 2.9. The figure shows that the Fano factors predicted by the GLM model had good agreement with the measured Fano factors, though slightly higher in general. A linear fit of the data revealed a slope of 1.2 for both white noise and texture. Therefore we can conclude that the model captured most of the fine structure within spike trains, though not entirely to the extremely repeatable level of the recorded data.

2.3.3 Timing precision of the model

Trigeminal ganglion neurons exhibit extremely high precision, on the sub-millisecond scale, in their spike timing under our experimental conditions as described in Section 2.3.1

Therefore it is fruitful to explore to what extent the GLM can reproduce this aspect of the response. As the model worked on discretized time bins, this set the limit of the precise timing correspondence between the stimulus and the resultant spike trains. We fitted models for the data at a range of time bin durations (0.125 ms to 10 ms) and calculated the prediction coefficients as before, which are summarized in Figure 2.10.

The GLM performed best with time bins of 1 ms to 2 ms, with the performance dropping off for both coarser and finer timing precisions. However, the models had a prediction quality coefficient of over 0.8 on the white noise stimulus across the range 0.5 ms to 4 ms. Under these experimental conditions, the neurons exhibited jitters in spike events around 0.25 ms, so the

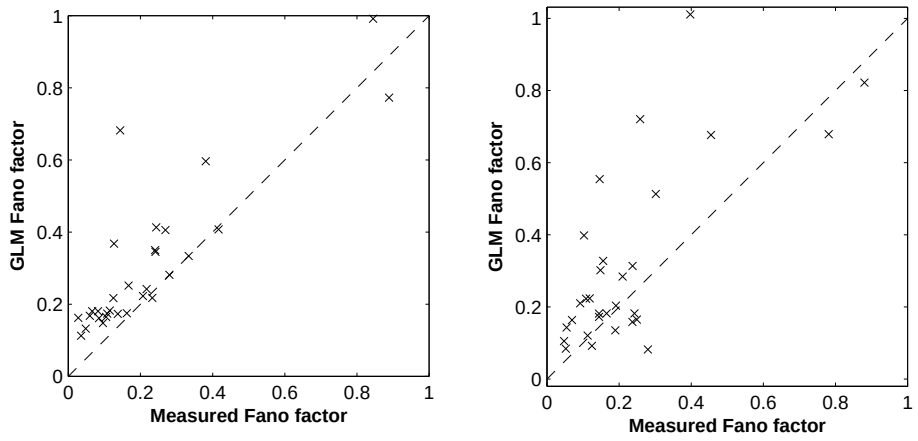

Figure 2.9: Fano factors for the model predictions against those calculated from measured spike trains. Left panel, white noise stimulus responses. Right panel, texture stimulus responses.

model came close to, but did not quite match, the timing precision found in this system.

The fact that performance drops at both fine and coarse timescales may be expected. When using longer time bins, information about the exact time of the spike is lost. If the neural code uses very precise timing, the model will not be able to reproduce the behaviour and predict the response of neurons to as high a degree as if this information was available. The fact that the prediction quality fell off for longer time bins indicates that this was the case: despite the seemingly easier task of predicting the response to a coarser timescale, the neurons (and models) were responding to much more temporally precise stimulus features. Conversely smaller time bins mean that the precise timing of spiking events must be predicted from the only information the model was given: the recent whisker position and spiking history. In the biological system, there are other factors, unavailable to the model. In particular, variations in the membrane potential on a sub-threshold level has persistent state that is not accounted for in the model. However, the whisker position had an autocorrelation time of 1.6 ms; it is therefore interesting that the model was capable of predicting the neural response at a finer precision than this.

One possibility for how the model was capable of reproducing the response down to such a fine timescale is given by the other input to the

model, the spiking history. We therefore also calculated the prediction coefficients for a model variant without spike history inputs across the same range of time bin widths. As Figure 2.10 shows, including spike history feedback in the model does not strongly affect the prediction quality above around 5 ms. This is likely because the timescale of refractoriness is on the order of a few milliseconds and so is unimportant for time bin widths of this size. At finer timescales the spike feedback was important for the accuracy of the model. For example, at the 1 ms time bin scale, the model with and without spike history feedback have median prediction coefficients of 0.92 and 0.78 respectively.

From these results, we may infer that what appears to be a restricting factor in the neurons' coding ability, refractoriness, actually has the effect of increasing spike train reproducibility. The jitter in spike timing we found was below that of the stimulus auto-correlation time, which would not be possible without some form of history dependence. This allows the highly temporally precise neural code as found in this system, with highly informative spikes.

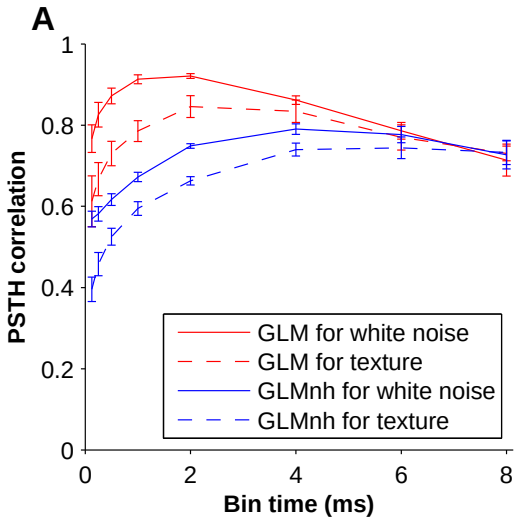

Figure 2.10: Timing precision of model predictions. Plotted are the median prediction quality coefficients across units as a function of time bin size. Results are shown for the full GLM and the GLM without spike history input (GLMnh), for both the white noise and texture stimuli. Error bars were calculated by bootstrap resampling (they are the standard deviation of 10000 new sets of coefficients generated by sampling with replacement from the original set of coefficients).

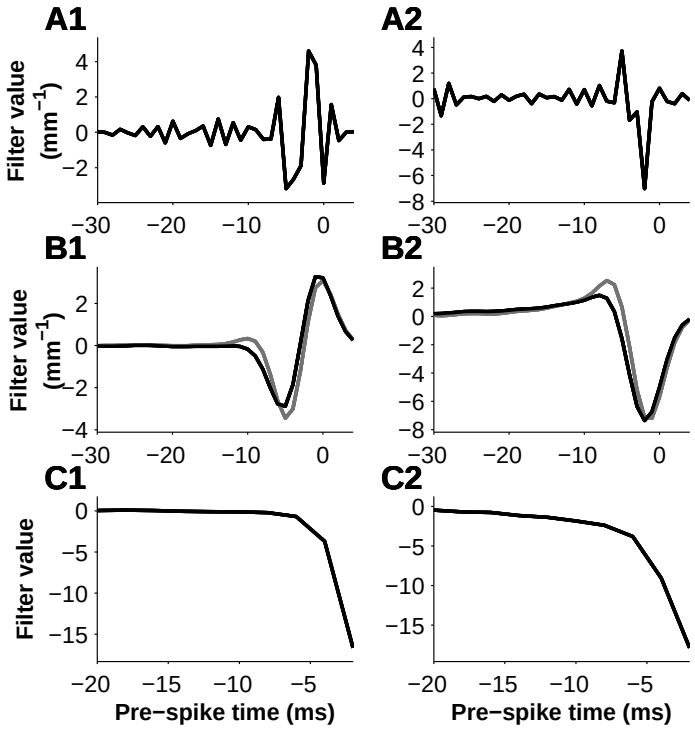

Figure 2.11: Example GLM fit for two cells (columns, as labelled **1** and **2**). **A**, Stimulus filter parameters $\vec{k}$. **B**, Stimulus filter convolved with the white noise autocorrelation (black line) compared with the unit's STA (grey line). **C**, The spike history filter $\vec{h}$.

2.3.4 Response characteristics of trigeminal ganglion neurons as accounted for by the model

The success of the model in predicting the response of the population of primary afferents to whisker stimuli suggested that we may gain useful insight into the coding properties of these neurons by examining the fitted parameters more closely. The parameters of the model class used to describe the response of the primary afferents can be split into three groups (see Section 2.2.5 for full details): b, the bias term that sets the spontaneous firing rate in the absence of any whisker stimulation, $\vec{k}$, the whisker stimulus filter that determines the stimulus feature to which the model is sensitive, and $\vec{h}$, the spike feedback filter that accounts for effects such as refractoriness. We can examine each of these in turn, for the individual neurons shown in Figure 2.11, before looking at their properties for the population as a whole.

The values of b for these two cells were -4.6 and -9.6 respectively, which correspond to spontaneous firing rates of $5\,\text{spike}\,\text{s}^{-1}$ and $0.03\,\text{spike}\,\text{s}^{-1}$.

The stimulus filters $\vec{k}$ for are shown in Figure 2.11 B1 and B2. These filters show that the neurons respond most strongly to precisely timed stimulus features, occurring 4 ms to 8 ms before a spike. This feature timing was quantified using the measure described in Section 2.2.7. The median feature delay for the population of neurons was -5.4 ms (IQR -7.2 ms to -4.1 ms).

The spike history filters (Figure 2.11 D1, D2) for these units were large and negative for recently occurring spikes. For spikes further in the past the filter value approached zero, showing that no effect of the spike history on the current response if the most recent spike was more than around 10 ms ago. This has the effect of enforcing a refractory period on the response; spikes are unlikely to occur only a few milliseconds apart.

Taken as a whole, we can see the picture that emerges from the GLM for these neurons: they exhibit very low firing rates in the absence of stimulation, responding strongly to temporally precise kinetic features of the stimulus with a strong, short refractory period.

2.3.5 Model parameters for the population

Having examined the model parameters for two particular example fits, we then went further to look at the population of recorded neurons as a whole. By investigating the variation and similarities between the fits, we wished to discover what our model tells us about the information encoded by the population of primary afferents.

The distribution of the values of b across all 34 recorded cells is shown in Figure 2.12. All of the values are negative, and most of them are large in magnitude; a value of -6.2 corresponds to a firing rate of approximately $1\,\text{spike}\,\text{s}^{-1}$ in the absence of a stimulus. Therefore the majority of model fits had values of b that corresponded to very low spontaneous firing rates (median $0.17\,\text{spike}\,\text{s}^{-1}$, IQR $0.01\,\text{spike}\,\text{s}^{-1}$ to $1.13\,\text{spike}\,\text{s}^{-1}$), matching well with the recorded data (median $0.04\,\text{spike}\,\text{s}^{-1}$, IQR $0.0\,\text{spike}\,\text{s}^{-1}$ to $0.14\,\text{spike}\,\text{s}^{-1}$), though somewhat higher. Note that this did not necessarily have to be the case: if the model were unable to explain the spikes evoked by the whisker stimulus, the value of b would be larger in order to increase the probability of these spikes occurring. The slightly higher spontaneous firing rates are likely due to this effect.

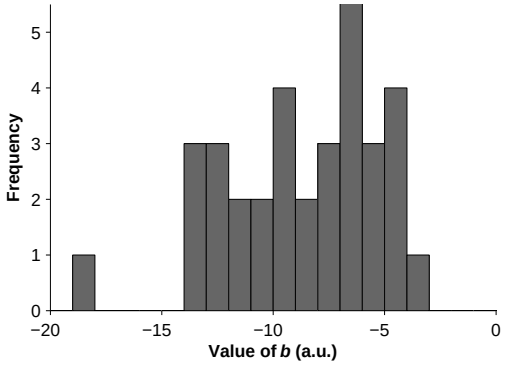

Figure 2.12: Histogram of the values of b for the population. The quartiles of the distribution were -10.8, -8.0 and -6.1, which correspond to spontaneous firing rates of $0.01\,\text{spike}\,\text{s}^{-1}$, $0.17\,\text{spike}\,\text{s}^{-1}$ and $1.13\,\text{spike}\,\text{s}^{-1}$

Across the population the form of the spike history filters was very simple. All units displayed a strong refractory effect shortly after a spike that gradually diminished over a timescale of around 10 ms. None of the units had positive feedback effects.

The most important aspect of the model from a sensory coding perspective is the stimulus filter. Given that the GLM framework explains the response of ganglion neurons to our dynamic whisker stimuli very well, what can we say about the information conveyed by the population? We investigated the stimulus feature space encoded by the cells using principal component analysis. Figure 2.13 shows the results of the analysis.

We found that the feature space could be largely described by only a small number of principal components: the first three principal components (shown in Figure 2.13 B1, B2, and B3) cumulatively accounted for 82 %, 94 % and 99 % of the variance. Therefore the stimulus selectivity of the recorded population of primary afferents can be accurately described by a low-dimensional "filter space". This filter space is visualized in Figure 2.13 C and D. In each panel, the filters are plotted at the value of their projection onto two of the principal components (the first and second in panel C, the first and third in panel D). The filters were evenly distributed across the filter space, "tiling" it. The implications of this are discussed in Section 2.4.3

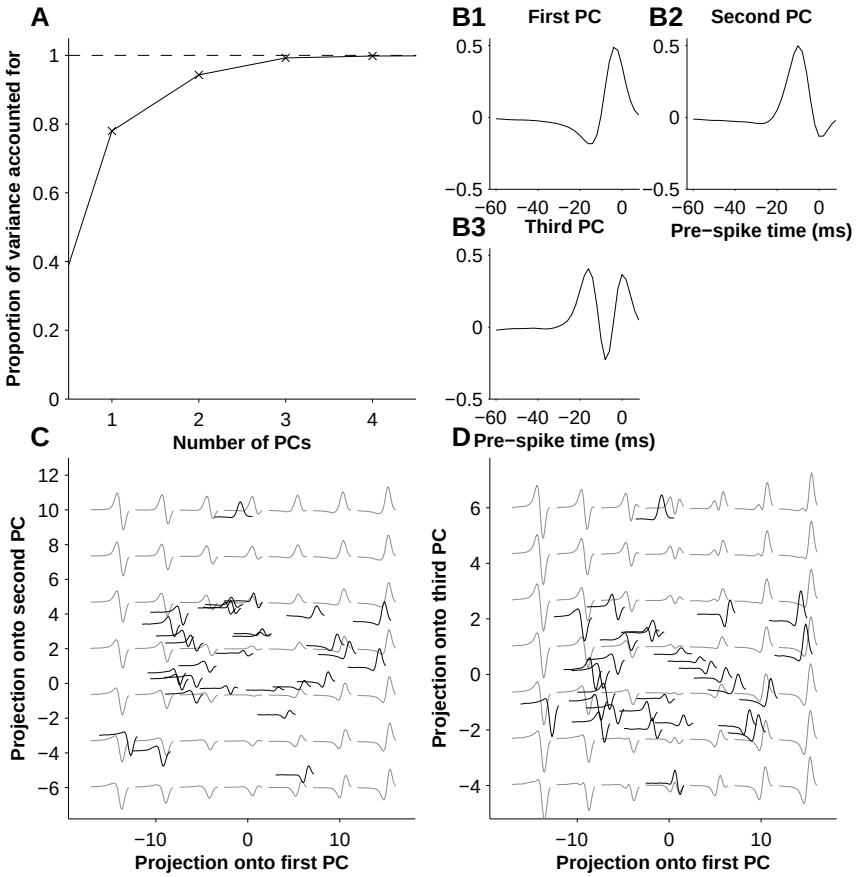

Figure 2.13: Stimulus feature space analysis. **A**, The cumulative variance accounted for by the first four principal components. **B1–3**, The first three principal components. **C**, The set of stimulus filters (black) projected onto the space spanned by the first two principal components. The space is visualized by showing in grey the features that would be formed by pure mixtures of the two components at those points. **D**, The set of stimulus filters (black) projected onto the space spanned by the first and third principal components. Again the stimulus features the space describes are plotted in grey.

2.4 Discussion

2.4.1 Predictive capability of the GLM

The GLM is one of the simplest model frameworks capable of describing count data such as that obtained by a spike-sorting electrophysiological approach. This comes with many advantages, the greatest being tractable parameter fitting and ease of interpretation. However, the simplifying assumptions have the potential to limit the predictive power of the model too much for many neural systems. For example, in barrel cortex neurons have been found to be best described using multi-dimensional nonlinear response function, as well as demonstrating other complexities in their behaviour, such as slow stimulus adaptation (Maravall et al., 2007; Lundstrom et al., 2010). In the case of the primary afferents measured in this study, the GLM was capable of predicting their response to a high degree of accuracy, both for a white noise stimulus similar to that used to fit the models and a texture stimulus, indicating a good level of generalization of the model and allowing confidence in the accuracy of its description. In addition, the GLM with spike history input maintained high prediction quality down to timescales below the autocorrelation time of the stimulus, recreating a widely-reported feature of the response of trigeminal ganglion neurons.

However, the prediction quality did degrade at the smallest timescales. In addition, the applied model framework is only capable of accounting for very simple adaptation effects. If we wished to account for such effects and model responses to very fine timescales, a model with state, persistent over time, would be necessary. Bio-mechanically inspired models have been used to successfully describe trigeminal ganglion neurons before (Mitchinson et al., 2004, 2008; Lottem and Azouz, 2011), but these models also have their drawbacks. The largest weakness of these models is that they contain a large number of free parameters, without an easy way to evaluate the likelihood of a response for any set of values of the parameters. This means parameter values must be tweaked by hand, a laborious and potentially bias-inducing procedure. Many of the advantages of the GLM can be retained with extensions to account for long timescale effects, some of which have been successfully applied in other neural systems (Paninski et al., 2009; Escola et al., 2011), but more work both theoretical and applied remains to make the most of the more sophisticated models.

2.4.2 Interpretation of the fitted models

Given that such a simple model had high predictive power under these experimental conditions, we infer that it is capturing real and important aspects of the neural code for this sensory system. As such, we can interpret the fitted model parameters to describe the coding scheme.

The recorded units responded to very temporally precise features, firing an action potential roughly 5 ms after the feature reached the firing threshold. Firing events were very temporally precise, which was facilitated by the fact that all units displayed a simple, strong refractory effect from previous spikes. Although this is biologically necessary given the mechanism of action potential firing, it is interesting that it also has the effect of increasing the timing precision of the system.

2.4.3 Stimulus encoding by the population

We found that it was possible to find a simple description of the feature space to which the population of primary afferents was responsive. A three-dimensional set of features could be used to capture 99 % of the variance in the neurons' filters, and the individual filters approximately tile the space. Combined with the varying firing thresholds in the different neurons, this means that each spike fired by a neuron narrows down the part of the space the stimulus is in significantly, i.e. conveys a lot of information.

In principle, the low-dimensional feature space means that just three neurons with linear output could convey the entirety of the encoded information. However, since neurons transmit information via action potentials this would require integration over long time periods in order to transmit the coordinate to a precise degree. This is at odds with the high temporal precision of this sensory system, and demonstrates the utility of the "over-complete" representation actually found in the population.

2.4.4 Possibilities for further work

Despite using a rich stimulus set compared with some previous work (e.g. "ramp-and-hold" stimuli), there are some simplifications. Firstly, the stimulus is only one-dimensional in space. It is known that trigeminal ganglion neurons are directionally selective (Zucker and Welker, 1969; Storchi et al., 2012), as well as highly sensitive to longitudinal whisker motion (Stüttgen

et al., 2008) and there is the possibility the response function in a directional stimulus space may have a more complex form.

Additionally, the recordings were taken from anaesthetized animals, eliminating the effect of active sensation. Although effects of attention should not be important at this stage in the sensory pathway, it is possible that motor control of the whiskers may influence the response characteristics of the neurons. Studies measuring neural activity in the whisker system during behaviour are now being performed and it should be possible to perform such studies with the trigeminal ganglion. One difficulty with such work is that it is impossible to deliver repeated stimuli, which means alternative methods of evaluating the performance of the model must be used.

The GLM provided a generally good description of the sensory code at this early stage of the pathway, which naturally invited the question of how we can use this information and these methods to investigate the transformation of the code at downstream areas of the brain. One of the major stages in the whisker sensory pathway is the ventro-posterior medial (VPM) area of the thalamus, and it is this area that is addressed in the next chapter.

Chapter 3

Changes in the neural code in the early stages of the whisker pathway are revealed by modelling

3.1 Introduction

A key feature of sensory systems, and the brain in general, is a hierarchical structure. In the previous chapter it was shown that it is possible to describe to a high degree of accuracy the response characteristics of the primary afferents of the whisker system, but in order to use the sensory information for complex behavioural tasks such as object identification it must undergo transformation. As described in Chapter 1, an important early stage in the whisker sensory pathway is the ventro-posterior medial (VPM) thalamus, which is the main afferent gateway into the somatosensory cortex.

Neurons in the VPM thalamus are organized into clusters, with a single cluster, known as a "barreloid", associated with each whisker. This is in contrast with the trigeminal ganglion, where evidence for somatotopic organization of whisker-innervating neurons is much weaker (Leiser and Moxon, 2006). There may also be an expansion in the number of neurons between the two stages of the sensory pathway: it is estimated that approximately 150 mechanoreceptors innervate each whisker in the rat whisker system, while barreloids contain around 250 neurons each (Lee and Woolsey, 1975; Land

et al., 1995). Additionally there are parallel pathways such as the "paralemniscal" pathway through the posterior nucleus of the thalamus that are less spatially specific. Given the change in anatomical conditions it could be expected that the neural code representing the whisker stimulus is different at this stage. The question naturally arises as to what processing occurs between the response of trigeminal ganglion neurons and thalamic neurons, and therefore in what form sensory information enters the somatosensory cortex and other brain regions. We will address this question using the same model-driven approach we used to explore the ganglion response in Chapter 2.

Previous work has also attempted to model the response of VPM neurons to explore the sensory code at this stage. Petersen et al. (2008) performed a study applying a white noise stimulus to a single whisker to obtain sensory features to which VPM neurons were responsive using STA and STC analysis. They found that an LNP model described the recorded properties well, describing the neurons as responsive to kinetic features of a timescale of 1 ms to 2 ms, with substantial diversity in the form of these features. They also found that significant minority of the neurons could not be adequately described by sensitivity to a single feature, requiring two or more dimensions in the stimulus representation to capture their response function. Using their LNP model, they were able to obtain a mean prediction coefficient (calculated by correcting the correlation coefficient by a method similar, but not identical, to the one used here) for the subset of units described as "single-feature" in response to white noise of 0.58 (SD 0.11). However, their model was only capable of predicting the PSTH as convolved with a Gaussian of SD 1.6 ms, a timing precision below that of the sub-millisecond spike timing that has been found in the system (Montemurro et al., 2007). We hope to improve on both the timing precision and overall prediction quality using our approach.

Also relevant to the modelling approach here is work by Montemurro et al. (2007), which used an information theoretic analysis to show (in a "model-free" manner) that most of the information in the VPM response to passive whisker stimulation could be accounted for by a neural code based on firing rate modulation on a sub-millisecond timescale, but that inter-spike correlations do also contribute some amount to the information carried by the code. Together with the results of Petersen (2007) showing that VPM

neurons are reliably responsive to linear kinetic features, this indicates that a GLM framework including spike history, may be able to describe the coding properties of VPM neurons to a higher precision than previous studies.

3.2 Methods

3.2.1 Electrophysiology

Recordings (performed by M. Bale) were taken from anaesthetized adult Wistar rats, ($n = 14$, urethane anaesthetic at $1.5\,\mathrm{g/kg_{body\ weight}}$) that were placed in a stereotaxic apparatus. The body temperature of the rats was maintained at 37.5 °C. A piezoelectric motor was used to insert a poly-electrode into the VPM thalamus. Extracellular recordings were amplified, sampled at 24.4 kHz and bandpass filtered (300 Hz to 3000 Hz).

3.2.2 Whisker manipulation

The whisker stimulus protocol was identical to that described in Section 2.2.2. Briefly, for each animal after electrode insertion the principal whisker was identified by manual stimulation before being inserted into a piezoelectric manipulator and stimulated in 50 epochs. Each epoch consisted of three 10 s sequences: a repeated texture stimulus, a repeated white noise stimulus, and a non-repeated white noise stimulus. The non-repeated white noise was used to fit model parameters, while the other two stimulus types were used to evaluate the model performance.

3.2.3 Spike sorting

Spike trains from individual units were obtained from the extracellular recordings using the same spike-sorting approach described in Section 2.2.3: first, 2 ms windows of the recorded potential were extracted whenever the potential crossed a threshold. The dimensionality of these windows was reduced using principal components analysis to 5, and clusters discovered by the fitting of a Gaussian mixture model. Units that did not exhibit a clear refractory period were discarded.

3.2.4 Unit selection

We wished to use only the most strongly responsive units identified by the spike sorting process, as many recorded units responded to the stimulus only weakly or not at all. One measure of how strongly a neural response is modulated by the stimulus is the mutual information between the stimulus and the response. Mutual information can be thought of as how much the uncertainty of one variable, e.g. the response, can be reduced by knowledge of another, e.g. the stimulus. It gives a measure of how well a model can perform in general. We used the method described by Strong et al. (1998) to calculate the information rate of recorded units from the PSTHs evoked by the repeated white noise stimulus. Only the most informative units (information rate greater than $5\,\mathrm{bit\,s^{-1}}$ for the white noise stimulus) were selected for further analysis, leaving a total of 36.

3.2.5 GLM fitting and evaluation

We used the same model framework, fitting methods, and prediction quality evaluation as described in Sections 2.2.5 and 2.2.6 in order to explore the sensory code of thalamus neurons.

3.3 Results

3.3.1 Properties of VPM response to whisker motion

In total, responses from 36 neurons from 14 animals were recorded and analysed. Consistent with results previously reported in the literature, the VPM responses to the applied white noise and texture stimuli were reliable and temporally precise, implying that the applied whisker stimulus contained features that are important to the sensory code. As shown in Figure 3.1, the white noise stimulus evoked a median firing rate of $4.9\,\mathrm{spike\,s^{-1}}$ (IQR $3.0\,\mathrm{spike\,s^{-1}}$ to $7.1\,\mathrm{spike\,s^{-1}}$), while the texture stimulus evoked a significantly lower firing rate on average ($p = 7.4 \times 10^{-4}$, Wilcoxon rank-sum test), with a median of $2.4\,\mathrm{spike\,s^{-1}}$ (IQR $1.2\,\mathrm{spike\,s^{-1}}$ to $3.9\,\mathrm{spike\,s^{-1}}$).

The jitter of the units was calculated using the same method as described in Section 2.2.4, and can be seen in Figure 3.1. There was no significant difference between the measured jitter in response to white noise and that in response to texture ($p = 0.20$, Wilcoxon rank-sum test), although it was

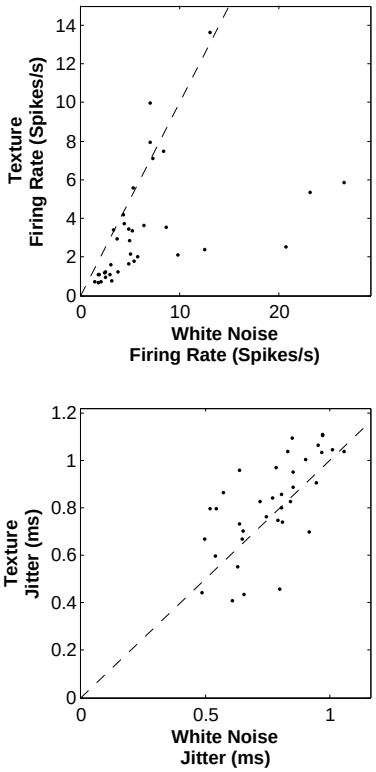

Figure 3.1: Some basic response characteristics of the thalamic neurons. Top panel: scatter plot of evoked firing rates for each unit for the texture stimulus against the white noise stimulus. Evoked firing rates are lower for the texture stimulus for a majority of units. Bottom panel: scatter plot of trial-to-trial variability in spike timing (jitter) for each unit for the texture stimulus against the white pnoise stimulus. Jitter is similar for the two stimuli.

slightly lower for white noise (median 0.80 ms, IQR 0.64 ms to 0.88 ms versus a median of 0.83 ms, IQR 0.70 ms to 0.98 ms for texture). These values are higher than those that were found in the ganglion, although still below the stimulus autocorrelation time.

In contrast with the PSTHs measured from ganglion neurons, the thalamic neurons were less consistent across trials. The thalamic neurons did not often reach the $> 90\,\%$ proportion of spikes in a bin that was found in the ganglion, more typically firing in around $60\,\%$ of trials at most. This was quantified by calculating the information rate from the PSTH, which can be thought of as a measure of its modulation as described in Section 3.2.4. The information rate calculated at 2 ms time precision for ganglion cells had a median of $47.8\,\mathrm{bit\,s^{-1}}$ (IQR $20.0\,\mathrm{bit\,s^{-1}}$ to $106.1\,\mathrm{bit\,s^{-1}}$), while the thalamic neurons, which already excluded units with an information rate less than $5\,\mathrm{bit\,s^{-1}}$, had a median rate of 9.0 (IQR $7.7\,\mathrm{bit\,s^{-1}}$ to $16.0\,\mathrm{bit\,s^{-1}}$). A Wilcoxon rank-sum test revealed this to be significantly different ($p = 5.3 \times 10^{-6}$). This clear difference confirmed that the thalamic responses are substantially less reliable under these experimental conditions than those in the ganglion.

Another measure was also calculated and found to corroborate these results: firing events were isolated by finding time bins in which a spike was found in over $10\,\%$ of trials and calculated the median of the spike frequencies in these firing events for each cell. For the ganglion the median of this measure across cells was 0.43 (IQR 0.32 to 0.68), indicating that if a neuron fired it tended to do so in a substantial proportion of trials. This is as opposed to the thalamic neurons where this measure was 0.15 (IQR 0.13 to 0.20), indicating that there were many firing episodes in which spikes occurred only in a much lower proportion of the trials. These results imply that the response of the thalamic neurons was not as predictable as that found in the trigeminal ganglion.

3.3.2 The GLM predicts thalamic responses

The GLM was fitted to each of the 36 recorded neurons using the non-repeated white noise stimulus. As with the ganglion response, we first asked how well the fitted models could predict the response of thalamic neurons to the repeated stimuli. Figure 3.2 compares model-predicted PSTHs for the two stimuli with the experimentally measured PSTHs, at a time resolution of

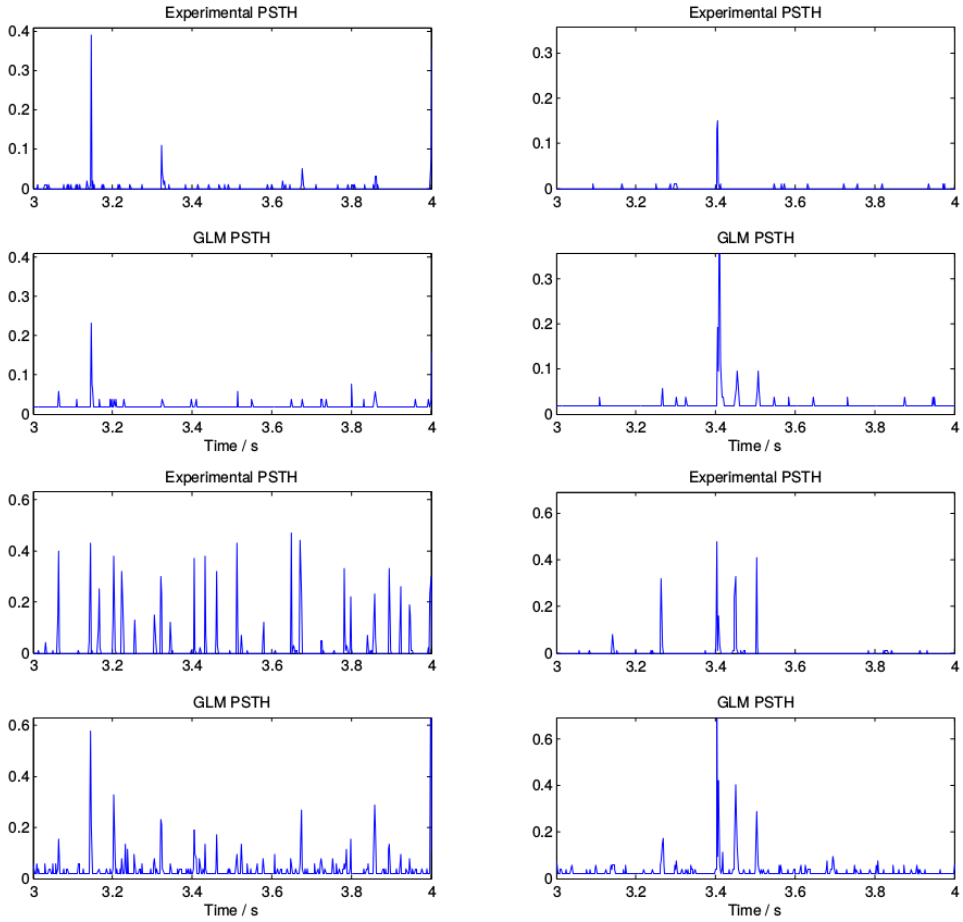

Figure 3.2: Example GLM PSTH predictions for two cells. Left column: responses from white noise stimulus. Right column: responses from texture stimulus. Rows from top to bottom: First cell experimental data, first cell GLM prediction, second cell experimental data, second cell GLM prediction.

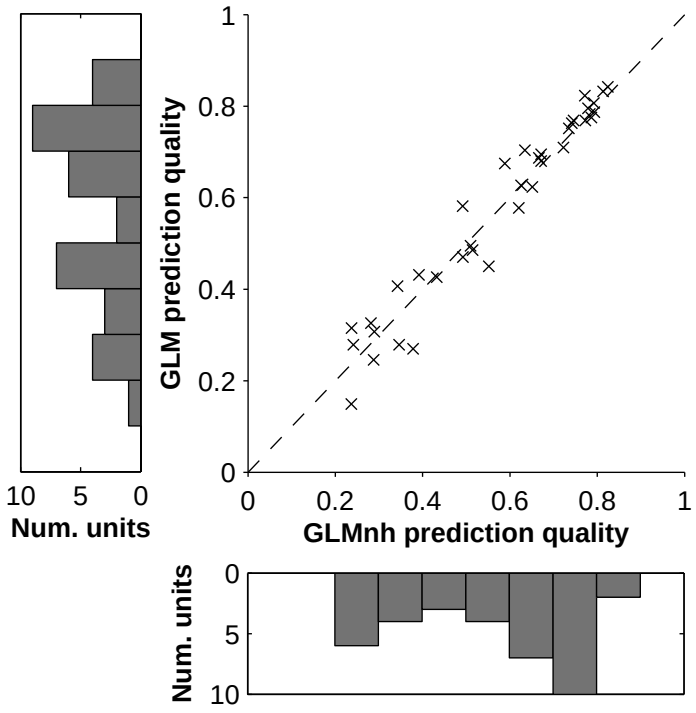

Figure 3.3: Scatter plot shows the prediction coefficients across the population of recorded VPM cells at 2 ms time resolution for white noise for the GLM against those for the GLM without spike history (GLMnh). The histograms show the quantity of units with prediction quality coefficients in bins with edges [0.0, 0.1, . . . , 0.9, 1.0].

2 ms. It can be seen that the model was capable of reproducing the majority of the strong response events at this timescale. This was true for both the white noise and texture stimuli, despite the sparser response to the latter.

We calculated the prediction quality coefficients as described in Section 2.2.6 for the population to quantify the model performance. Figure 3.3 summarizes the prediction quality coefficients for the fitted models, both with and without the influence of spike feedback. The median coefficient for the white noise stimulus was 0.63 (IQR 0.42 to 0.77), while for the texture stimulus it was 0.57 (IQR 0.41 to 0.67). The GLM therefore does capture a substantial portion of the modulation in the responses as measured by the PSTH.

Influence of spike feedback

Figure 3.3 compares the prediction quality coefficients for the sets of GLMs fitted with and without spike history effects. The median prediction quality coefficients for the model without spike feedback for the white noise and texture stimuli were 0.62 (IQR 0.38 to 0.74) and 0.55 (IQR 0.38 to 0.68) respectively. Including spike feedback had no significant effect on the quality of the models (for white noise stimulus, $p = 0.88$, for texture stimulus $p = 0.89$, Wilcoxon rank-sum test). This was in contrast to the results for the ganglion, where it was shown that including spike history strongly improved the model, especially at finer timescales.

3.3.3 Interpreting the GLM fits

Figure 3.4 shows the model fits for two example units. The units responded to precisely timed features, which typically depended on stimulus features around 10 ms before a spike. A measure of the position of the filter relative to the response, as described in Section 2.2.7 had a median of −10.1 ms (IQR −12.6 ms to −8.8 ms).

The spike history filters no longer had the simple refractory form found in the ganglion. This may indicate different firing modes such as bursts or other inter-spike correlations. For example, comparing the spike history terms in Figure 3.4 the second fit showed essentially a simple refractory effect while the first had a strongly excitatory effect for spikes occurring 2 ms to 6 ms in the past. However, given that the inclusion of spike feedback did not improve model performance (see Figure 3.3), it is difficult to read too much into this difference from the ganglion.

We repeated the fitting and evaluation procedure for each neuron across a range of time bin widths (0.125 ms to 10 ms) to test how well the model captured the precise spike timing of the system. The results are shown in Figure 3.5. The median of the coefficients was best for white noise at a timescale of 2 ms but remained above 0.5 in the range 1 ms to 6 ms. For the texture stimulus the median was lower for shorter timescales but higher at the longer timescales.

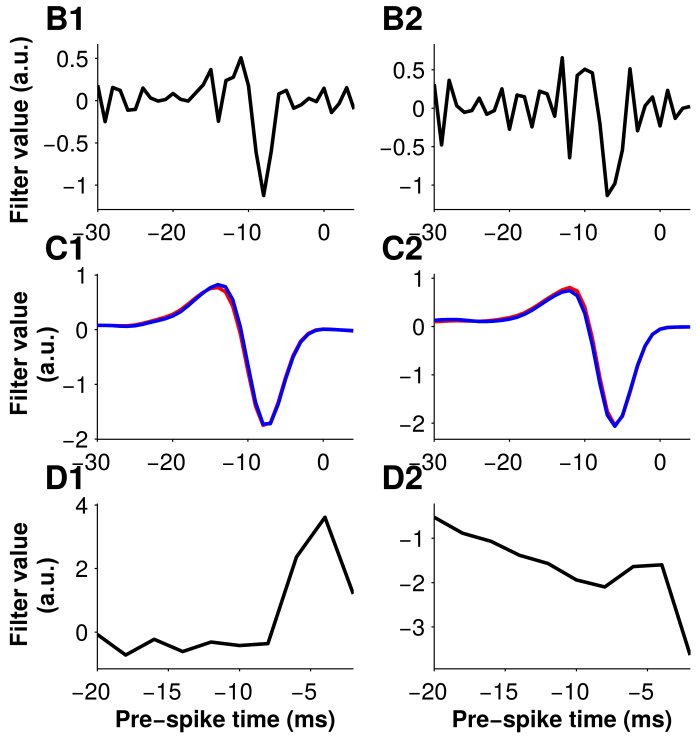

Figure 3.4: An example GLM fit for two cells (columns, as labelled **1** and **2**). **B**, Stimulus filter parameters $\vec{k}$. **B**, Stimulus filter convolved with stimulus autocorrelation (blue) and STA (red). **D**, Spike feedback filter $\vec{h}$.

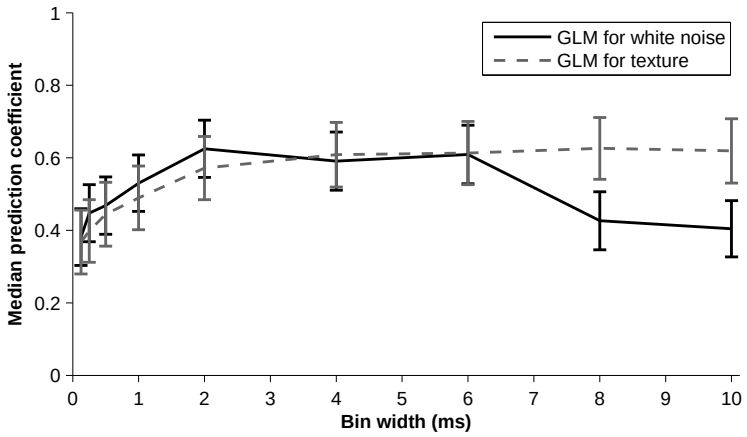

Figure 3.5: The median prediction coefficients across cells for the GLM across a range of time bin widths for both the white noise and texture stimuli. Error bars are standard errors on the median as calculated by bootstrap resampling.

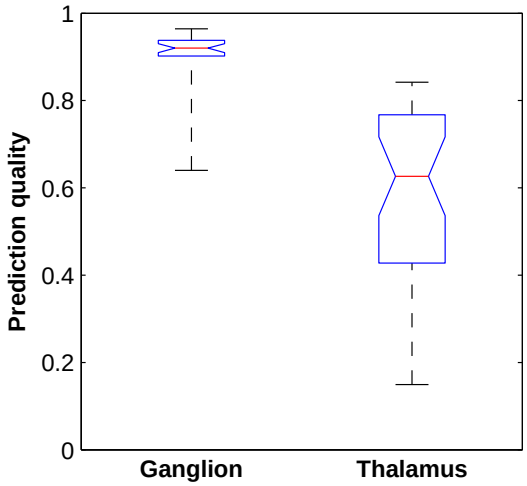

Figure 3.6: Box and whisker plot of thalamus GLM prediction quality vs ganglion GLM prediction quality. Box borders are the first and third quartiles (containing therefore 50% of the data), with the median shown by the red horizontal line

3.3.4 Comparison with ganglion results

Although a significant fraction of the recorded thalamic neurons were quite well predicted (19 of the 36 had prediction quality coefficients above 0.6 for white noise, for example), Figure 3.6 shows that the prediction quality coefficients for the recorded population of thalamic units were lower than that for the ganglion. In fact, the best predicted thalamic unit was worse than the first quartile for the ganglion. Although as noted before the thalamic neurons did not respond as consistently to the stimulus across trials, this should be corrected for to an extent in the prediction coefficient calculation. Therefore a more likely explanation for the disparity is that there are one or more aspects of the thalamic response not captured by the GLM as applied here.

3.4 Discussion

As the GLM framework was very successful in accounting for the response properties of trigeminal ganglion neurons as shown in Chapter 2, we applied

a similar methodology to data gathered from the VPM thalamus, another early stage in the whisker sensory pathway.

As reported previously in the literature, VPM neurons responded reliably and with fine temporal precision: the trial-to-trial variability in timing was measured at less than 1 ms. This is remarkable considering that even the white noise stimulus had an autocorrelation time of 1.6 ms

However, the response of thalamic neurons was less robust than that of ganglion neurons in general. This has clear implications for the predictability of the response, and may be worth investigating further in its own right. From the perspective of the experimenter, the variability is seen as noise, but additional information in the brain may give the context needed to make use of the differing response to similar stimulus conditions.

3.4.1 Describing the VPM thalamus response

The stimulus filters of the GLM were temporally precise and spikes were evoked around 10 ms after the appearance of a feature.

In contrast to the ganglion, the spike feedback filters displayed a variety of effects. Some filters had excitatory terms for recently occurring spikes, which caused the model to display "bursting" behaviour, a firing mode commonly found in thalamic neurons (Sherman, 2001). This can be linked to results by Montemurro et al. (2007), which attributed a small but consistent amount of information in the VPM spike trains to the effect of bursts. However, the inclusion of the spike feedback terms did not improve model performance, which would seem to show that the simple linear feedback effect of past spikes in the GLM is not entirely adequate to explain the effects of inter-spike correlations in the VPM.

We can compare the strength of the model description with the results of Petersen (2007). In their study the predicted responses a STA-fitted LNP models were compared with measured PSTH responses that were convolved with a 1.6 ms Gaussian, with the resulting prediction quality coefficients having a mean of 0.58. This can be compared with the results presented above, of prediction quality coefficients with a median of 0.63 at the 2 ms timescale. Due to differences in methodology, the results can not be directly compared, but they do seem to indicate broadly similar levels of performance. This is impressive given that the model they used was more flexible than the GLM here, having a fitted non-monotonic tuning function.

Petersen (2007) also found that a subset of VPM neurons they recorded were not adequately described by a single-dimensional stimulus filter and needed two or more features to explain their response characteristics. This may help to explain why the GLM was not as successful in predicting responses in VPM units as it was in the primary afferents of the trigeminal ganglion. As the greater trial-to-trial variability is corrected for to some extent by the calculation method of the prediction quality coefficients, we expect that at least some of this gap should be possible to bridge. In other words, there were some aspects of the thalamic sensory code that were not captured by the GLM, despite its partial successes. We therefore examined some of the assumptions implicit in the GLM framework in order to make improvements to better describe the sensory code at this stage.

3.4.2 Examining the assumptions of the model

Why was the GLM framework applied here less successful in explaining the thalamic sensory code than the code of the trigeminal ganglion? A good way to address this question is to explore the assumptions of the model, where they might fail, and how they might be relaxed.

Probably the most important assumption is that the thalamic neurons respond monotonically to single linear features of the stimulus in the stimulus basis described by whisker position. Even though we have shown that this assumption worked well for ganglion cells, the sensory information likely undergoes transformation for further use in the brain. It is certainly possible that the signal is transformed enough by the point of the thalamic case that the linear representation of whisker motion is no longer adequate.

Fortunately, there are many well-explored methods for introducing nonlinear feature dependencies in both the GLM and related model frameworks. For example, it is possible to remain within the GLM framework while "augmenting" the representation of the stimulus space with higher-order polynomial terms, such as quadratics. It would also be possible to transform the stimulus features in a different way - one well-justified possibility would be to put the stimulus through GLMs fitted on ganglion data. Another possibility is a model framework with adaptive basis functions, the most prominent of which is the Multi-Layer Perceptron (MLP), a neural network model. In this model framework, it is possible to automatically "discover" basis transformations that are effectively fed into a GLM, similar to what we used in

this chapter, as new input.

3.4.3 Going beyond GLMs

A major advantage of the GLM is ease of interpretation. However, we have seen that despite its successes in describing the thalamic response, it is not as effective as it was for the ganglion data. It is possible that the spike trains are simply less predictable, but given that we use a prediction quality metric that corrects for this to some extent, it is more likely that the model is deficient in certain respects. Important effects may have been missed, so we moved to a more sophisticated model with nonlinear multi-feature sensitivity with the aim of adequately capturing the sensory code in the thalamus.

Chapter 4

Going beyond GLMs improves understanding of the thalamic sensory code

4.1 Introduction

The results presented in the previous chapter showed that a generalized linear model framework was capable of predicting and explaining important aspects of the neural response in the VPM thalamus, matching or improving on previous modelling attempts in the literature. However, the predictive power of the model for the thalamic neural population can be contrasted with the corresponding results presented in Chapter 2 for the trigeminal ganglion, where prediction quality coefficients were much higher. Although the responses recorded in the thalamus were less reproducible than those measured in the trigeminal ganglion, this is corrected for to some extent in the calculation of the prediction quality coefficient, leading to the conclusion that there is significant room for improvement in the accuracy of modelling the response.

Section 3.4.2 outlined some of the potential changes in modelling approach that could yield improvements in the prediction of the thalamic response, and therefore hopefully in understanding the form of the sensory code. A simple and justifiable modification to the modelling approach that may yield improvements is a transformation of the stimulus representation. That is, there is little reason to believe that the stimulus representation

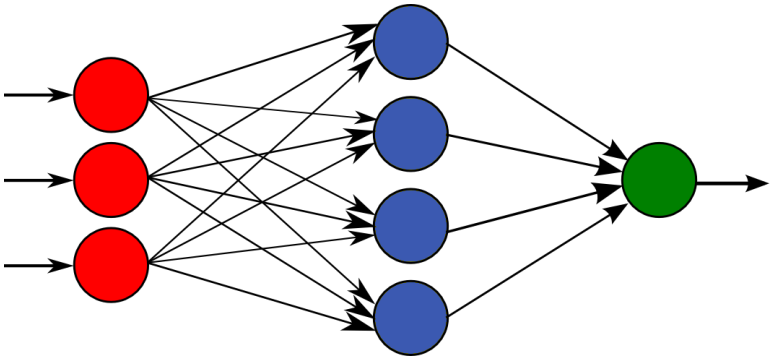

Figure 4.1: A schematic representation of an MLP model. The red set of nodes are set to the input values for each data point. The blue set forms the "hidden" layer that apply linear-nonlinear functions to the inputs. The green node again performs a linear-nonlinear computation to produce the output, which in our case indicates probability of the presence of a spike.

provided to the model (i.e. the recent history of whisker position) is a good one to explain the encoding behaviour of the neurons. The position representation did work well for the trigeminal ganglion, but if some non-trivial processing occurs in the generation of VPM spikes, that will no longer be the case. An appropriate change in the basis in which the stimulus is represented will improve the model by taking into account nonlinear stimulus dependencies of the firing patterns.

A very important factor in successful statistical modelling is appropriate feature selection; that is, representing the inputs to the model in a way that allows simple computations to reproduce the output. As such, a major strand the modelling literature concerns finding ways to automatically uncover such representations. There are many approaches to this problem, including augmenting the stimulus matrix $\mathbf{X}$ with nonlinear terms (Park, 2011) and non-parametric methods such as Gaussian processes (Rasmussen and Williams, 2006). Each approach has its own advantages and disadvantages in generality, computational tractability, interpretability, and other desiderata.

An important modelling approach with many similarities to GLMs is the Multi-Layer Perceptron (MLP), a form of feed-forward neural network. They are an evolution of simpler biologically-inspired models such as the perceptron (Rosenblatt, 1958), and can easily be cast into a probabilistic form very similar to that used for GLMs. MLPs first came into prominence

after the back-propagation algorithm for model fitting was discovered by Rumelhart et al. (1986). Described more fully in Section 4.2.1, their structure is similar to stacked layers of GLMs, where the output of each layer is used as input for the next, as shown in Figure 4.1. During the fitting process of the models, the hidden layers "learn" new feature representations of the data which are passed on to subsequent layers, which allows the model to represent arbitrary nonlinear functions (Cybenko, 1989).

Since the output of the trigeminal ganglion is well described by a population of GLMs, this model framework is a natural progression. Although it can sometimes be difficult to interpret the action of MLPs, this class of model is well studied and has been successfully applied in many domains, including neuroscience. Feed-forward neural networks have been used to study and describe neurons with nonlinear stimulus-response transformations such as those in V1 (Lau et al., 2002; Prenger et al., 2004).

We therefore decided to use this model class to attempt to describe the VPM thalamus neural code as it is more powerful than the GLM, with the capability to model the nonlinear, multiple-feature stimulus dependencies that seemed to be present in these neurons. A substantial improvement in the predictive power of the model would then confirm that there is some aspect of the coding schema not described by the GLM, and not present in the trigeminal ganglion, that may be interpreted.

4.2 Methods

4.2.1 Mathematical framework of MLPs

We limited our analysis to neural networks with a single hidden layer. Each unit in the hidden layer is similar to the GLM as described in Section 2.2.5, different in that the output is not used as the spiking probability. Instead, the output is fed into another unit whose output determines the probability of a spike. The output of the hidden layer with m units is given by

$$z_j = f\left(\vec{k_j}^\intercal \vec{x} + \vec{h_j}^\intercal \vec{n} + b_j\right),$$

where $j = 1, \ldots, m$ indexes the hidden units. z_j is the output of unit j. All other notation is the same as for the GLM. The time indices of the inputs and output have been omitted for clarity. The final probability of a spike, π

is the given by the output unit, described by the equations

$$a = \vec{w}^{\intercal}\vec{z} + c,$$

$$p\left(r = 1|\theta, \vec{x}\right) = \pi = f\left(a\right),$$

where k indexes output units and the parameters of the output unit are $\vec{w}$ and c, and θ stands for all model parameters. c plays the same role as the bias as for the GLM, essentially setting the spontaneous firing rate, and $\vec{w}$ controls how strongly the output of the MLP depends on the output of each hidden unit. The full likelihood is given by using the Bernoulli distribution:

$$\log p(\vec{r}|\theta, X) = \sum_t r_t\pi_t + (1 - r_t)(1 - \pi_t) \tag{4.1}$$

where we have restored the time indices on the right hand side to make explicit that π_t is unique for each time bin.

Note that output of the hidden units is essentially a transformed (and reduced dimension) representation of the initial input. In order to keep the model simple while still allowing a useful nonlinear representation, we used MLPs with a single hidden layer composed of three units.

In a similar way as for the GLM, we used a Gaussian prior for the parameters. The only difference in this case is that the parameters were separated into more different groups with different scale hyperparameters. The groupings used were the hidden layer stimulus filter weights $\vec{k_j}$, the hidden layer spike history filter weights $\vec{h_j}$, and the output layer weights $\vec{w}$. The final expression for the log-prior is therefore:

$$\log p(\theta|\alpha, \beta, \gamma) = \frac{1}{2}\left[\alpha\sum_{i=1}^{M}\|k_i\|_2^2 + \beta\sum_{i=1}^{M}\|h_i\|_2^2 + \gamma\|w\|_2^2\right] \tag{4.2}$$

The models were trained with the same Maximum *a Posteriori* method used for the GLM. That is, the expression given by the addition of Equations 4.1 and 4.2 (the log-posterior) was maximized with respect to the parameters. In the context of neural networks, this is often referred to as the "backpropagation" algorithm, as errors from the output unit are propagated backwards to the hidden units to calculate gradients and curvatures of the likelihood. We again used the evidence procedure to find good hyperparameters for the MLP (MacKay, 1992).

4.2.2 Feature space analysis

The method we used to analyse the feature space the MLP model found was similar to that described in Section 2.2.8. That is, a principal component analysis was applied to the set of model stimulus filter vectors, and the relevant subspace defined as that defined by the principal components accounting for 95 % of the variance in the filters. There was a slight difference in that each model had three stimulus filter vectors. These were simply treated together, so that the matrix $\mathbf{K}$ had $3 \times$ num. neurons $= 108$ rows.

4.3 Results from the modeling changes

The MLP models were fitted using the same data as in Chapter 3: 3000 s of white noise stimulation spike train data for each VPM neuron ($n = 36$).

It was important to evaluate the level of improvement that the model brings to our understanding of the neural response. We have already seen that a GLM was able to capture a substantial portion of the thalamic behaviour (see Chapter 3), so there needs to be significant improvement in the prediction quality to make up for the drawbacks of a more complex model. We therefore began by qualitatively and quantitatively evaluating the performance of the MLP model in comparison with the GLM approach.

4.3.1 Moving to non-linear stimulus selectivity improves prediction accuracy

We first looked at the prediction quality coefficients across the population for the white noise stimulus, shown in Figure 4.2. We found that the model performance improved for nearly all cells compared with the GLM. As reported in Chapter 3, the GLM achieved a median performance of 0.63 (IQR 0.43 to 0.77), while the median prediction coefficient for the MLP was 0.80 (IQR 0.70 to 0.88). Improvements were also seen in the prediction of the texture response, as shown in Figure 4.3. The points in the scatter plot are nearly all above the line of equality, indicating better predictive performance of the MLP, some substantially so. The median coefficient for the GLM was 0.57 (IQR 0.43 to 0.68), against 0.70 (IQR 0.59 to 0.76) for the MLP. The difference between the predictive power of the different models was statistically significant in both cases ($p = 3.4 \times 10^{-5}$ for white noise, 0.003 for

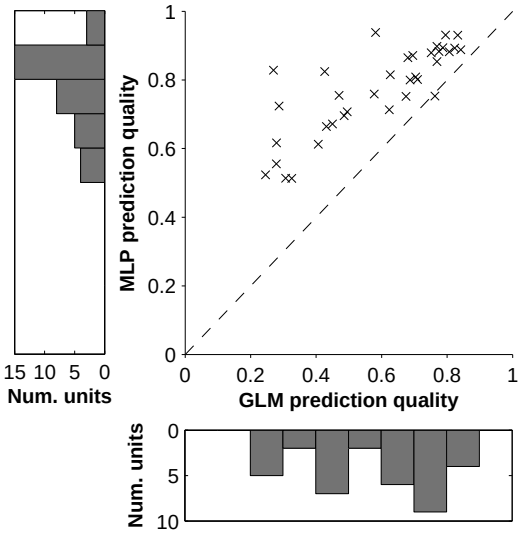

Figure 4.2: Scatter plot of prediction quality coefficients obtained from the white noise stimulus for the MLP against those for the GLM. Histograms along the axes show the frequency of units falling in bins with edges [0.0, 0.1, . . . , 0.9, 1.0].

texture, Wilcoxon rank-sum test). The MLP models clearly more accurately reproduced the spiking behaviour of VPM neurons, indicating that it is capturing some aspect of their spiking behaviour not described by the fitted GLMs.

4.3.2 Interpreting the model improvements

We wished to obtain an understanding of how the MLP models were able to better predict the PSTHs, by examining some individual examples of improved models. First, we looked at an example of generated spike trains to the repeated stimuli, as shown in Figure 4.4. It can be seen that the thalamic response exhibited robust, temporally precise spiking events as described in Chapter 3, with little firing outside of these events. In contrast, the GLM showed quite noisy behaviour with much greater trial-to-trial variability. This can be seen particularly clearly in the response to the texture stimulus. There, the measured spike train shows only around six firing events in the figure. Outside of these events, there are only a few isolated spikes over the one hundred trials. In contrast, although the GLM does reproduce

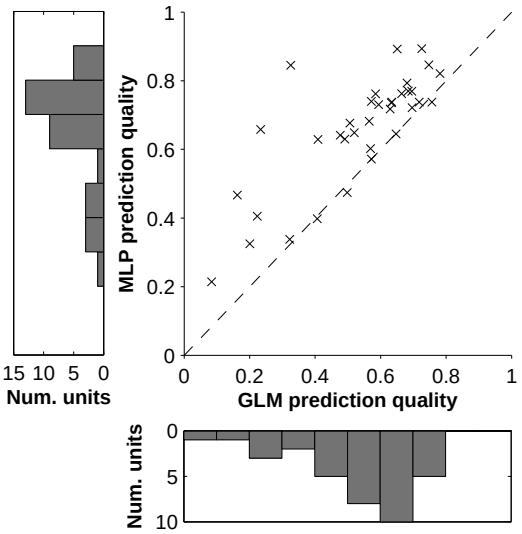

Figure 4.3: Scatter plot of prediction quality coefficients obtained from the texture stimulus for the MLP against those for the GLM. Histograms along the axes show the frequency of units falling in bins with edges [0.0, 0.1, . . . , 0.9, 1.0].

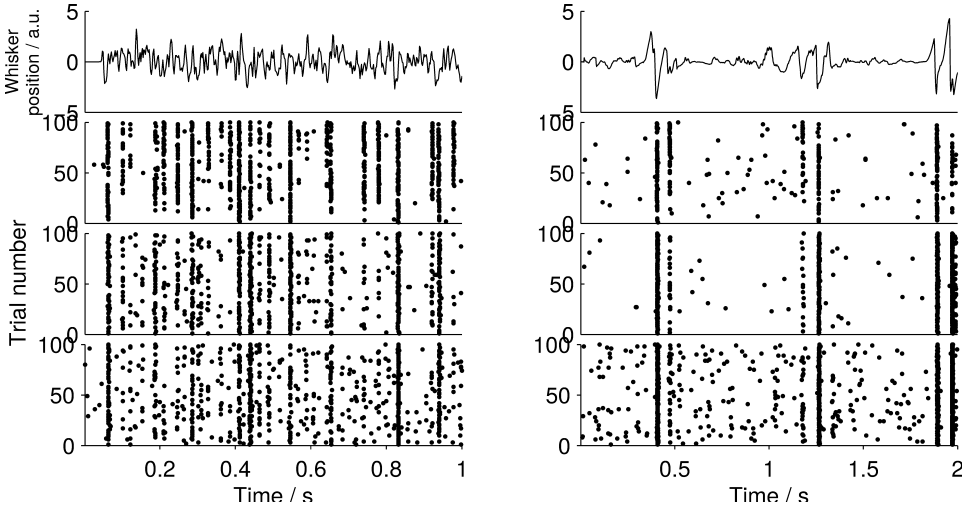

Figure 4.4: Comparison of recorded spike trains with those generated by the GLM and MLP models for an example unit. The top row shows the applied stimulus, which in the left column is a section of the repeated white noise stimulus, and in the right column a section of the texture stimulus. The second row shows the recorded spike trains, the third row the simulated MLP spike trains and the bottom row the stimulated GLM spike trains. There were 100 trials in each case.

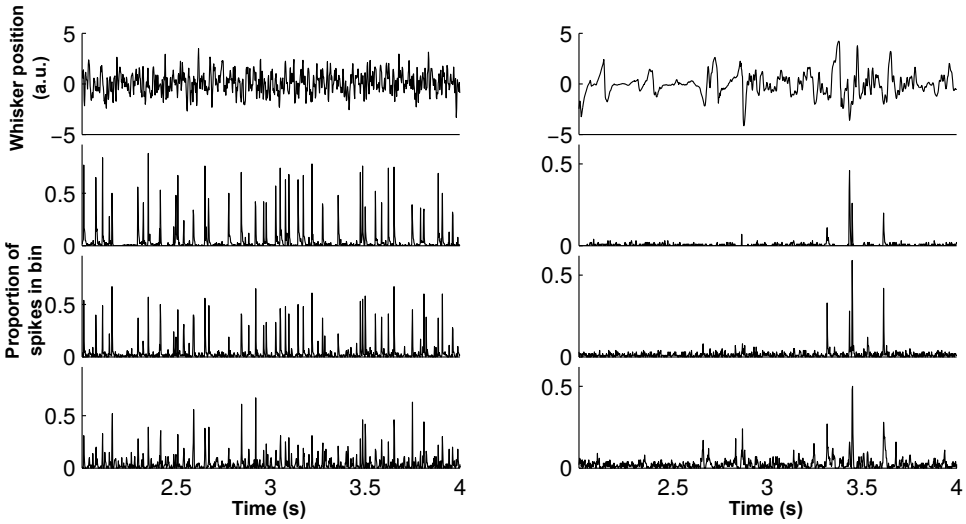

Figure 4.5: Comparison of recorded response to repeated stimuli for an example unit (different from the one shown in Figure 4.4). The first row shows the applied whisker stimulus: white noise for the left column, texture for the right. The second row shows the recorded PSTH, the third the MLP model simulation, and the bottom row the GLM simulation.

the firing events with good fidelity, outside of these events there are many individual spikes. The MLP model improved on this, with less variability between trials in the quiet periods. In response to the white noise a similar pattern can be seen, with the MLP model exhibiting lower across-trial variability. Despite this, the MLP prediction does not seem to quite reach the same reproducibility of the recorded response.

Another representation of the response to repeated stimuluation is the PSTH, examples of which are shown in Figure 4.5. Similar differences in the predictions as in Figure 4.4 can also be seen here. For example, in the GLM's predicted response to the texture stimulus, there are many small peaks that are not found in either the real neuron's response or the MLP model prediction, again due mainly due to the greater trial-to-trial variability in the quiet periods in the neural response. It can also be seen in the white noise response in Figure 4.5 that although the GLM does often reproduce spiking events, the MLP model captures the amplitude of these events to a better degree of accuracy.

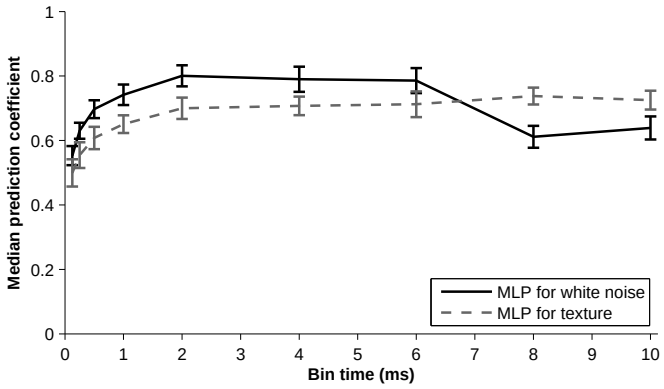

Figure 4.6: Timing precision of MLP model predictions. The median prediction quality coefficients across the population of recorded units are plotted as a function of the spike bin size. Error bars are calculated as the standard error on the median using bootstrap resampling.

4.3.3 Model performance across the scale of spike train timing precisions

Previous work modelling the spiking behaviour of VPM neurons was only able to predict PSTHs which had been convolved with a Gaussian distribution with a standard deviation of 1.6 ms (Petersen, 2007). The GLM performed reasonably well, achieving similar predictive accuracy without smoothing. However, as previously reported in the literature VPM neural responses are precise to a sub-millisecond timescale and a significant amount of information is encoded by spike timing (Montemurro et al., 2007). We wished therefore to explore how well the MLP model could predict the response of the population of recorded units across a range of spike timing precisions. To this end, the models were fitted across a range of time bin widths (0.125 ms to 10 ms) and the prediction quality coefficients calculated for each case.

The results for the white noise stimulus are summarized in Figure 4.6, which plots the median prediction quality coefficients against time bin widths. The best quality predictions were found at the 2 ms timing precision, in common with the GLM of Chapter 3. However, as already noted, the coefficients calculated from the MLP model predictions were significantly higher than those from the GLM predictions. This was also the case for the smaller time bin widths, and even for the smallest time bin (0.125 ms) the performance

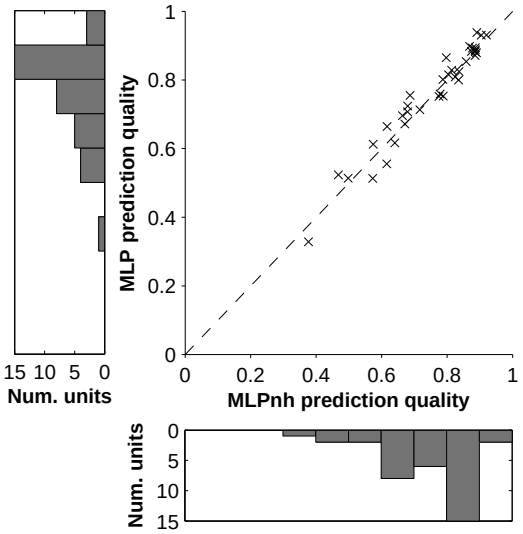

Figure 4.7: Scatter plot of prediction quality coefficients obtained from the white noise stimulus for the MLP without spike feedback against those for the MLP.

of the MLP was similar to that of the GLM at 1 ms (medians 0.55 and 0.53 respectively). The MLP model therefore was able to reproduce to a much greater degree of fidelity the spiking behaviour of the thalamic neurons at these fine timescales.

4.3.4 Effect of spike history feedback

The results in Section 3.4.1 showed that the spike history filters no longer had the simple refractory form that was found in the ganglion, and also did not improve the predictive capabilities of the models. The possibility remained that a model capable of representing more complex relationships between stimulus sensitivity and inter-spike correlations would find more useful structure in this area. However, as shown in Figure 4.7 for the white noise stimulus at 2 ms timing precision, this was not borne out by the results and the MLP model performance was not improved by including spike history. This was true for both stimuli at all timing precisions. The implications of this are discussed in Section 4.4.

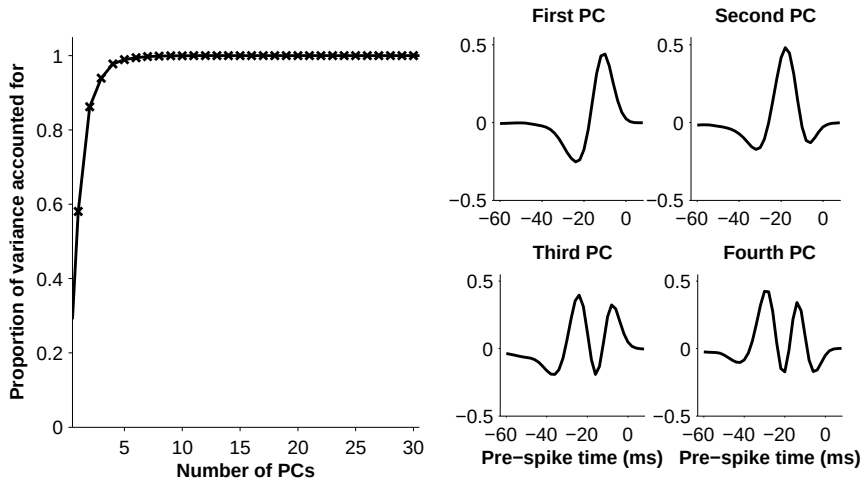

Figure 4.8: The results of the principal components analysis on the set of hidden layer stimulus filter parameters. Left panel: cumulative proportion of variance accounted for by the principal components. Right panels: the first four principal components.

4.3.5 Stimulus feature selectivity of the population

The MLP model proved to be more accurate in predicting the responses of VPM thalamus neurons than any previous study of this system. We therefore wished to see what the model could tell us about the stimulus features encoded by the thalamic population. This is more difficult than for the GLM framework, as in that case the stimulus filters entirely describe the features that excite firing in the model. In the MLP model, the stimulus filters are combined nonlinearly and therefore describe a nonlinear manifold of stimulus space. In other words, hidden layer units could represent inhibitory features or be part of a compound excitatory feature. Nevertheless, we applied a similar analysis of the feature space represented by the learned stimulus filters of the hidden layer units in the same way as we did for the ganglion GLM filters.

The method is described fully in Section 4.2.2, but briefly, a principal component analysis was applied to the set of stimulus filters, the results of which are shown in Figure 4.8. The left panel shows how much variance was cumulatively accounted for by the principal components, which can be compared with the results obtained for the similar analysis on the GLM stimulus filters for the trigeminal ganglion. There, the first three principal

components accounted for over 99 % of the variance in the stimulus filters. To reach that level for the VPM filters required six components, and four were required to account for over 95 % of the variance. Therefore the feature space which VPM neurons were differentially responsive to was in some sense larger than the space we found in the trigeminal ganglion data.

The first four principal components, which accounted for over 95 % of the variance in the stimulus filters are shown in the four right-hand panels of Figure 4.8. Qualitatively, they seem similar to those calculated from the GLMs of trigeminal ganglion in Chapter 2; the first two closely resemble ideal velocity and acceleration features, while the next two describe kinetic features involving higher-order derivatives of whisker position.

4.4 Discussion

We found in Chapter 3 that although the GLM successfully described many aspects of the VPM thalamus response to whisker stimulation, there was clear room for improvement. We therefore decided to employ a more powerful model, the multilayer perceptron, to capture the encoding properties of these neurons. We found that the MLP modelling framework resulted in substantially better performance at predicting the response of VPM neurons to dynamic whisker stimuli than GLMs, across the whole range of spike timing precisions.

The modelling accuracy results can be compared with previous work done in the VPM thalamus. In particular, the LNP model used by Petersen (2007) achieved a mean prediction coefficient over a set of 36 neurons of 0.58 (SD 0.11). The results presented here therefore represent a substantial improvement, as this level of performance was achieved to a timescale of 0.25 ms, while the median prediction quality coefficient reached over 0.8 for a time bin width of 2 ms. It is also important to note that the results of Petersen (2007) were calculated after the measured spike trains had been convolved with a Gaussian of width 1.6 ms, which makes for a considerably easier problem than prediction with millisecond scale time bins.

4.4.1 Coding properties of VPM neuons

A qualitative evaluation of the predictions revealed a few noticeable differences between the predictions of the GLM and MLP models relative to the

recorded results. First, the contrast between firing events and quiet periods was clearer in the MLP predictions, which were closer to the experimental results in that outside of intense firing events there was very little activity. Second, the MLP more accurately reproduced the scale of the firing events themselves. A thorough explanation of how the neural network model was able to achieve this is difficult, but a possible interpretation is that the sensory code at this stage has transformed such that the neurons' excitatory stimulus features are no longer linear in the whisker position basis. The GLM fits were able to find the linear direction in the stimulus space in which neurons were responsive, and thus account for a substantial portion of the spiking response, but unable to account for nonlinear variations within this region, which could include locality, for example. These coding results corroborate with those found by Petersen (2007), being similar in several respects. First, the stimulus features were found to have high temporal resolution. The results in this chapter go beyond those of Petersen et al., as due to methodological constraints they were only able to resolve the features to a timescale of around 2 ms, while the MLP model found features capable of predicting the response on a sub-millisecond timescale. Second, they found diversity in the form of feature selectivity, with the response not being explained by velocity sensitivity alone, for example. This is confirmed and expanded upon by the results presented in Figure 4.8, where we found that six kinetic features were required to describe 99 % of the variance in the stimulus filters of the model. Third, they found that a subset of neurons could not be described by single feature sensitivity. The improvement in predictive performance of the MLP models over the GLMs confirms this, but also suggests that the view of only a subset of neurons having this behaviour is incorrect, as the improvement in performance was seen in nearly all of the recorded neurons.

4.4.2 Non-stationarity in the neural response

One notable feature of the thalamic response that was not accounted for in any of the models presented is non-stationarity, an example of which is shown in Figure 4.9. This figure shows a raster plot of spikes, with clear horizontal bands of high and low activity periods, which could be explained by switches between stimulus-responsive and unresponsive states. That is, at different times the unit appeared to respond to different features, or respond

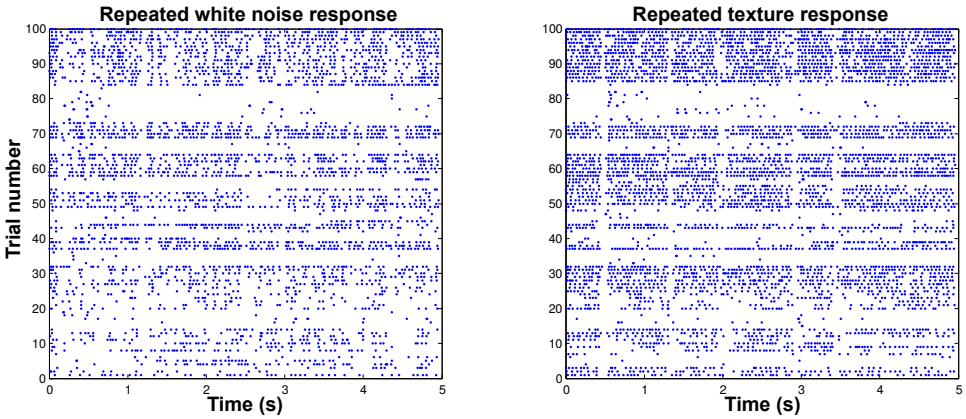

Figure 4.9: Raster plot of a thalamic unit's response to 50 repititions of a white noise stimulus. Clear banding in the response shows that this unit has distinct firing states.

with different intensity, and this behaviour was common across most of the recorded VPM neurons.

As shown above, the thalamic response displays changes in firing state that cannot be accounted for by the models in their current state. This not only means that the model predictions will correspond less well to the experimental data, but that the model fit will also be affected negatively. For example, if the neuron switches between stimulus-dependent and stimulus-independent states, the model fit will be somewhere between these states, being less strongly driven by the stimulus than the neuron in its stimulus-dependent state, but more strongly than in the independent state. This would mean the model does not properly capture the behaviour of the neuron in either state.

Non-stationarity in the neural response also has some important methodological implications; if the response characteristics change over trials, the PSTH no longer represents all of the information contained in the spiking responses to repeated trials. To account for this kind of behaviour, it would be necessary to move to a model with an internal state, able to describe and reproduce long time-frame changes in neural response properties. Potential methods for dealing with these issues are discussed in Chapter 5.

4.4.3 Conclusion

The multilayer perceptron framework was able to describe the behaviour of VPM thalamus neurons to a high degree of fidelity, surpassing the performance of previous models presented in the literature. In terms of coding properties, it seems the more powerful model was necessary to accurately describe the VPM thalamus. This is evidence that there is transformation in the neural code even at these early stages of the sensory pathway. Although the coding mechanism is similar to that found in the trigeminal ganglion in that it consists of spikes of high timing precision in response to kinetic features of the stimulus, the kinetic features to which it responds were found to be more complex. Additionally, there was evidence of different types of spike correlation and varying network state.

Chapter 5

Conclusion

In this thesis we have applied rigorous modelling techniques in order to explore and explain the sensory code of two of the early stages of the rat whisker sensory pathway. We have shown that it is possible to predict the response of neurons in the trigeminal ganglion and VPM thalamus to dynamic whisker stimulation using statistical modelling techniques and examine the resulting models to gain insight into the coding properties of these neurons.

5.1 The generalized linear model revealed that the primary afferents form a highly informative overcomplete basis

Generalized linear models have a very simple structure that is conducive to parameter fitting and interpretation. They proved to be a very good framework for describing the responses of trigeminal ganglion neurons, which respond very precisely and mostly monotonically to single kinetic stimulus features. The good performance of the models enabled us to interpret the parameters to find an intuitive coding interpretation of the population of trigeminal ganglion neurons. Here, we discuss these findings in the context of previous research into whisker-related trigeminal ganglion neurons.

An important aspect of the study was the use of complex time-varying stimuli, specifically white noise and texture. Classical studies in the trigeminal ganglion system used simple stimuli, often ramp-and-hold whisker deflections, where the whisker is deflected to a certain angle and held there for a relatively long period of time (tens of milliseconds or more). These

studies discovered some important aspects of the responses of the whisker primary afferents, including their remarkable sensitivity to small deflections (Gibson and Welker, 1983) and their tuning properties with respect to deflection parameters such as direction, (Lichtenstein et al., 1990), velocity, and position (Shoykhet et al., 2000). These early studies often categorized the neurons as Slowly Adapting (SA) or Rapidly Adapting (RA) depending on whether they showed a tonic response to sustained deflection or not. However, the simple stimulus ensembles meant that the exact features to which the neurons responded could not be extracted. This was the motivation for moving to complex stimulus ensembles, in particular white noise stimuli, that explore much more of the possible stimulus space.

In common with our findings, Jones et al. (2004b) showed that complex stimuli, specifically low-pass filtered white noise stimuli, elicited highly reproducible responses from trigeminal ganglion neurons. They also found that the categorization of the neurons as RA or SA had no predictive power with respect to the similarity of spike trains across trials. In another paper (Jones et al., 2004a) they used a linear encoding model to successfully infer the whisker stimulus that evoked a given spike train; however, they did not provide a model of spike generation to account for the characteristics of the neurons' responses.

Some work since then has taken a mechanically-inspired approach (Mitchinson et al., 2008; Lottem and Azouz, 2011), combining an integrate-and-fire neuron model with a simple mechanical model representing the dynamics of the follicle-sinus complex. These models were successful in predicting the responses of neurons to an array of stimulus types, but had the serious drawback that all of the parameters required hand-fitting. Not only is this laborious, but it also increases the flexibility of the model, reducing the generality of the conclusions that can be drawn from its fit.

There are always trade-offs in modelling decisions. The approach taken here was of a simple and relatively inflexible model with automatically fitted and regularized parameters. Despite this, we found a very good correspondence between the fitted models' predictions and the measured spike trains, increasing our confidence that the model was capturing the important aspects of the neural code under these experimental conditions. We were then also able to provide an explanation of the coding strategy of the trigeminal ganglion in terms of features of whisker motion. We found the features en-

coded by the neurons formed an over-complete basis of a low-dimensional feature space, where each spike from an individual neuron is highly informative about where we are in the stimulus space.

5.2 The sensory code undergoes transformation in the early stages of the pathway

The success of the GLM in predicting the response of primary afferents indicates that the sensory code of these neurons can be accurately described by linear filtering. When applying the model framework to the VPM responses, however, the limitations of the linear model became apparent. We found that a model capable of representing nonlinear stimulus dependencies, the multi-layer perceptron, achieved much more accurate predictions, indicating that the response of VPM neurons to the applied stimuli is more complex and only partially captured by linear filtering.

We can compare the results found here with the work of Petersen et al. (2008). Using a similar white noise whisker stimulation paradigm, they measured spike trains from individual VPM thalamus neurons and analysed the results using an LNP model. They were able to achieve predictions of similar to quality of those produced by the GLM here, and as such the two studies can draw some similar conclusions: VPM neurons encode these stimuli with precisely-timed spikes on the basis of diverse kinetic features of whisker motion. Importantly, they also found a subset of neurons not well described by their single-feature LNP model, but whose spiking behaviour was modulated within a higher-dimensional space.

Petersen et al. (2008) did not provide a model to characterize these multi-feature neurons, but the nonlinear multiple feature selectivity they found agrees with our findings that moving to a more powerful model, the multilayer perceptron, yielded improved predictive capability. However, we found that the MLP improved on the GLM predictions for a large majority of the measured neurons, indicating that although the simpler models did describe important aspects of the sensory code, it was inaccurate to describe only a subset of the neurons as multi-feature selective. The modelling extensions needed to explain the response of VPM neurons showed that these neurons respond to more complex features of whisker motion than the trigeminal ganglion, and that even at this early stage in the sensory pathway

the neural code is already undergoing some degree of transformation.

We can put this in additional context with the work of Bale and Petersen (2009): using a directional ramp-and-hold stimulus paradigm, they found that responses became less reliable and less informative along the sensory pathway from ganglion to VPM and somatosensory cortex, and concluded that the neural code is transformed from a highly precise temporal code in the trigeminal ganglion to a more rate-based code in the somatosensory cortex. This conclusion may be disputed, however, due to the simple stimulus applied: if the thalamus and cortex have a more complex stimulus-response function, as we have found here, the ramp-and-hold stimuli may simply not be among the neurons' preferred stimuli, resulting in the less reliable response. Despite this, their findings do agree with ours in that the neural code has already changed between the trigeminal ganglion and the thalamus.

5.3 Relevance of precise spike timing

Our understanding of how the early stages of sensory pathways encode information has progressed greatly since the seminal work of Adrian (1926). His experiments showed that the intensity of a sensory stimulus could be encoded by the rate of action potentials emitted by a sensory neuron. However, in a behavioural context, animals need to make decisions based on sensory information quickly and without the benefit of repeated trials. In these circumstances the concept of "firing rate" is ill-defined and important changes in the environment may occur on a timescale in which only a few spikes could possibly be emitted. Additionally, the information theoretical argument of MacKay (1952) showed that a spike train can transmit exponentially more information with increasing timing precision. On this basis, it has long been recognized that neural codes making use of precisely timed spikes may exist. However, experiments in various sensory systems, such as the visual cortex in response to a moving grating (Tolhurst et al., 1983) and the auditory nerve in response to pure tones (Teich and Khanna, 1985) found that the mean and variance of the spike count in response to a stimulus were approximately equal, consistent with Poisson-like firing statistics. This led to the view that neurons could only support a neural code based on the aggregation of spikes over relatively long timescales.

Contrary to the view of neurons as relatively noisy coding elements, how-

ever, results such as those of Segundo et al. (1963) and Mainen and Sejnowski (1995) using injected current stimulation of cells *in vitro* showed that under many conditions, spike generation is a largely deterministic process that can correlate with stimuli on a millisecond timescale. The time of propagation of action potentials was also shown to be precise on such timescales (Lass and Abeles, 1975). These results indicated that codes using individual spike timing are biophysically possible.

The seeming contrast between the noisy coding found in earlier experiments and the precision of the biophysical mechanisms was reconciled when it was recognized neurons code more reliably under more natural stimulation. This has been demonstrated in many different systems (Miller and Mark, 1992; de Ruyter van Steveninck et al., 1997) and confirmed again by the results in this thesis. Each sensory modality has its own constraints imposed by the mechanism of transduction, yet, it seems a general feature of primary afferents that they operate very close to the physical limits on the timing of spike generation (Rieke et al., 1999; Bialek, 2002).

5.4 Modelling approaches for understanding neural coding

As methods for gathering neural data have improved, the need for and value of sophisticated analytical methods has increased. In this thesis we have demonstrated the effectiveness of probabilistic modelling techniques for understanding the coding properties of the early somatosensory system of the rat. Despite the success of the models, there remain many relatively unexplored directions for improving their explanatory power.

One immediately apparent aspect of the modelling that can be altered according to need is the input to the model. For example, in this thesis we used a spike feedback mechanism for single neurons, but it is possible to extend this to allow inter-neural connections in regions of the brain where this is expected (Paninski et al., 2007), or to treat the spikes of one population of neurons as input to another (Babadi et al., 2010). A related approach is to include pre-synaptic neural activity explicitly in a model as an unobserved variable to be inferred (Kulkarni and Paninski, 2007).

Another important choice is the selection of prior for the parameters. It is possible to think of this as another hyperparameter of the model, one

that we can optimize. In this thesis we used a relatively simple, widely used prior, the spherical Gaussian distribution, though within the context of a Type-II maximum likelihood procedure. This procedure finds a scale for the model parameters that optimizes the marginal likelihood of the hyperparameters and thereby increases the predictive power and interpretability of the fits. However, more sophisticated priors are possible, for example Park and Pillow (2011) explored a Type-II maximum likelihood procedure they called "Automatic Locality Determination" (ALD), which used a prior capable of capturing the tendency for sensory receptive fields to be localized, in both time and frequency. They found that this form of prior increased the accuracy of model fits in simulations involving a wide variety of simulated stimulus filter types and also greatly reduced the amount of data required to find a good fit for experimental data.

We can also consider how to treat the output of neurons. It was assumed for all models in this thesis that the relevant unit of the neural code is the single spike. There is evidence in the whisker system that at the thalamic level codes that distinguish between different firing patterns, e.g. bursting and tonic firing, carry more information than those only considering single spikes (Montemurro et al., 2007). This may not be a problem if the model is sophisticated enough to account for and generate similar complex spike patterns, which may be the case for models with spike feedback and nonlinear stimulus dependencies. Otherwise it could be necessary to differentiate between firing patterns and treat them as different categories of output from the system.

Section 4.4.2 showed that the response properties of VPM neurons were not stationary, possibly switching states between different stimulus dependencies. Therefore it would make sense to more explicitly model long-term (on the order of seconds) dependencies. Two promising frameworks for this kind of modelling are hidden Markov models and recurrent neural networks. Hidden Markov models, also known as "state-space" models, have seen some use in the neural coding problem in recent years (Brown et al., 1998; Paninski et al., 2009), but recurrent neural networks have not seen much use despite recent advances in overcoming fitting difficulties, such as those by Martens and Sutskever (2012) and Monner and Reggia (2012).

There are clearly many directions in which the modelling of neural sensory coding in the rodent whisker system and sensory systems in general

could be expanded and refined. It can be noted, however, that two major concerns in modelling, accuracy and interpretability, are often at odds; it is often possible to construct a sophisticated model with great predictive accuracy that is nevertheless difficult to use to aid scientific understanding. The extent to which this is true and how much of a problem it is remains debated, but on a practical level it reminds us to keep in mind what use we intend to make of our models. When selecting a modelling approach we should be always carefully consider what use we wish to make of them and how they can aid our understanding.

5.5 Directions for future research in the rat whisker system

As noted above, there remain many potentially fruitful avenues of research in terms of applying powerful modelling techniques to neural systems in general. Here we note some directions for research into the rat whisker system in particular.

5.5.1 Making recordings in awake animals

All data in this thesis were obtained from anaesthetized animals using externally applied whisker stimuli. This has clear experimental and analytical advantages such as exact control over whisker motion, allowing repeated stimulus trials. This was the basis for most evaluation of model performance in the analysis, and as we have shown this approach can give insight into the sensory code. However, this level of control over conditions also takes the experiments away from the more natural conditions for which the code evolved. For all sensory modalities motor control of sensory apparatus is important, and perhaps particularly so for the sense of touch. Therefore it is likely that recordings from behaving animals will become more common and more important in the future. There may also be concerns over the potential effect of anaesthesia on the behaviour of neurons, which becomes more important further along the pathway, particularly in cortex. Experiments using awake animals would avoid this difficulty.

Work in this area is in progress; for example O'Connor et al. (2010) studied some of the coding properties of barrel cortex neurons in head-

fixed mice performing an object localization task, though without taking a modelling approach. This new paradigm does bring its own difficulties in applying such an approach: several techniques used in this paper, e.g. the prediction quality coefficients, required the precise repeated application of a stimulus. However, the modelling framework remains applicable, and retains the advantages when using natural stimulation over classical reverse correlation techniques.

5.5.2 Making use of data from deeper in the sensory pathway

In this thesis we gathered and analysed data from some of the earliest stages of the rat whisker sensory pathway, and found an active role in sensory processing being played by the thalamus. As the sensory information enters the cortex, anatomical conditions change drastically. As discussed in Chapter 1, there is a massive increase in the number of neurons associated with each whisker, estimated at 10 000 per barrel column. It is likely that neurons in the barrels are responding to compound features involving input from other whiskers and the motor system. As even in the thalamus a more powerful model than the GLM improved response predictions, careful consideration of the modelling approach must be taken in the cortex. Experimentally, it is important to find and apply stimuli that will reveal the coding properties of cortical neurons and allow accurate predictive models to be fitted. These issues poses challenges, but also opportunities for finding good descriptions of sensory representations and move towards a more complete understanding of neural coding in general.

Bibliography

E. Adrian. The impulses produced by sensory nerve endings. *The Journal of physiology*, 61(1): 49, 1926. ISSN 0022-3751. URL http://jp.physoc.org/content/61/1/49.full.pdf.

E. Ahissar, R. Sosnik, and S. Haidarliu. Transformation from temporal to rate coding in a somatosensory thalamocortical pathway. *Nature*, 406(6793):302–6, July 2000. ISSN 0028-0836. doi: 10.1038/35018568. URL http://www.ncbi.nlm.nih.gov/pubmed/10917531.

K. Alloway. Information processing streams in rodent barrel cortex: the differential functions of barrel and septal circuits. *Cerebral Cortex*, 18(5):979, May 2008. ISSN 1047-3211. doi: 10.1093/cercor/bhm138. URL http://cercor.oxfordjournals.org/cgi/content/abstract/18/5/979.

K. D. Alloway, M. Zhang, and S. Chakrabarti. Septal columns in rodent barrel cortex: functional circuits for modulating whisking behavior. *The Journal of comparative neurology*, 480(3):299–309, Dec. 2004. ISSN 0021-9967. doi: 10.1002/cne.20339. URL http://www.ncbi.nlm.nih.gov/pubmed/15515173.

M. L. Andermann, J. Ritt, M. a. Neimark, and C. I. Moore. Neural correlates of vibrissa resonance; band-pass and somatotopic representation of high-frequency stimuli. *Neuron*, 42(3):451–63, May 2004. ISSN 0896-6273. URL http://www.ncbi.nlm.nih.gov/pubmed/15134641.

E. Arabzadeh, R. S. Petersen, and M. E. Diamond. Encoding of whisker vibration by rat barrel cortex neurons: implications for texture discrimination. *The Journal of neuroscience : the official journal of the Society for Neuroscience*, 23(27):9146–54, Oct. 2003. ISSN 1529-2401. URL http://www.ncbi.nlm.nih.gov/pubmed/14534248.

E. Arabzadeh, E. Zorzin, and M. E. Diamond. Neuronal encoding of texture in the whisker sensory pathway. *PLoS biology*, 3(1):e17, Jan. 2005. ISSN 1545-7885. doi: 10.1371/journal.pbio.0030017. URL http://www.ncbi.nlm.nih.gov/pubmed/15660157.

E. Arabzadeh, S. Panzeri, and M. E. Diamond. Deciphering the spike train of a sensory neuron: counts and temporal patterns in the rat whisker pathway. *The Journal of neuroscience : the official journal of the Society for Neuroscience*, 26(36):9216–26, Sept. 2006. ISSN 1529-2401. doi: 10.1523/JNEUROSCI.1491-06.2006. URL http://www.ncbi.nlm.nih.gov/pubmed/16957078.

B. Babadi, A. Casti, Y. Xiao, E. Kaplan, and L. Paninski. A generalized linear model of the impact of direct and indirect inputs to the lateral geniculate nucleus. *Journal of Vision*, 10(10):1–14, 2010. ISSN 1534-7362. doi: 10.1167/10.10.22.Introduction. URL http://www.journalofvision.org/content/10/10/22.full.

M. R. Bale and R. S. Petersen. Transformation in the neural code for whisker deflection direction along the lemniscal pathway. *Journal of neurophysiology*, 102(5):2771–80, Nov. 2009. ISSN 1522-1598. doi: 10.1152/jn.00636.2009. URL http://www.ncbi.nlm.nih.gov/pubmed/19741100.

M. R. Bale, K. Davies, O. J. Freeman, R. a. a. Ince, and R. S. Petersen. Low-Dimensional Sensory Feature Representation by Trigeminal Primary Afferents. *Journal of Neuroscience*, 33 (29):12003–12012, July 2013. ISSN 0270-6474. doi: 10.1523/JNEUROSCI.0925-13.2013. URL http://www.jneurosci.org/cgi/doi/10.1523/JNEUROSCI.0925-13.2013.

G. R. Belford and H. P. Killackey. Vibrissae representation in subcortical trigeminal centers of the neonatal rat. *The Journal of comparative neurology*, 183(2):305–21, Jan. 1979. ISSN 0021-9967. doi: 10.1002/cne.901830207. URL http://www.ncbi.nlm.nih.gov/pubmed/500854.

M. Berry and M. Meister. Refractoriness and neural precision. *The Journal of neuroscience*, 18 (6):2200, Mar. 1998. ISSN 0270-6474. URL http://www.jneurosci.org/content/18/6/2200.short.

W. Bialek. Thinking about the brain. *Physics of Biomolecules and Cells*, May 2002.

M. Brecht and B. Sakmann. Whisker maps of neuronal subclasses of the rat ventral posterior medial thalamus, identified by whole-cell voltage recording and morphological reconstruction. *The Journal of Physiology*, 538(2):495, 2002. ISSN 0022-3751. doi: 10.1013/jphysiol.2001.012334. URL http://jp.physoc.org/content/538/2/495.short.

E. Brown, L. Frank, D. Tang, and M. Quirk. A statistical paradigm for neural spike train decoding applied to position prediction from ensemble firing patterns of rat hippocampal place cells. *Journal of Neuroscience*, 18(18):7411–25, Sept. 1998. ISSN 0270-6474. URL http://neuro.cjb.net/cgi/content/abstract/18/18/7411.

G. Carvell and D. Simons. Biometric analyses of vibrissal tactile discrimination in the rat. *Journal of Neuroscience*, 10(8):2638, 1990. URL http://www.jneurosci.org/cgi/content/abstract/10/8/2638.

G. E. Carvell and D. J. Simons. Task- and subject-related differences in sensorimotor behavior during active touch. *Somatosensory motor research*, 12(1):1–9, 1995. URL http://www.ncbi.nlm.nih.gov/entrez/query.fcgi?cmd=Retrieve\&db=PubMed\&dopt=Citation\&list_uids=7571939.

E. J. Chichilnisky. A simple white noise analysis of neuronal light responses. *Network (Bristol, England)*, 12(2):199–213, May 2001. ISSN 0954-898X. URL http://www.ncbi.nlm.nih.gov/pubmed/11405422.

G. Cybenko. Approximations by superposition of a sigmoidal function. *Mathematics of Control, Signals, and Systems*, 2:303–314, 1989. URL http://scholar.google.com/scholar?hl=en\&btnG=Search\&q=intitle:Approximations+by+superposition+of+a+sigmoidal+function\#4.

R. R. de Ruyter van Steveninck, G. D. Lewen, S. P. Strong, R. Koberle, and W. Bialek. Reproducibility and variability in neural spike trains. *Science (New York, N.Y.)*, 275(5307):1805–8, Mar. 1997. ISSN 0036-8075. URL http://www.ncbi.nlm.nih.gov/pubmed/9065407.

A. Dean. The variability of discharge of simple cells in the cat striate cortex. *Experimental Brain Research*, 44(4):437–440, 1981. ISSN 0014-4819. URL http://www.springerlink.com/index/KU31781R04161752.pdf.

M. E. Diamond. Texture sensation through the fingertips and the whiskers. *Current opinion in neurobiology*, 20(3):319–327, Apr. 2010. ISSN 1873-6882. doi: 10.1016/j.conb.2010.03.004. URL http://www.ncbi.nlm.nih.gov/pubmed/20403683.

M. E. Diamond and E. Arabzadeh. Whisker sensory system - from receptor to decision. *Progress in neurobiology*, 103:28–40, Apr. 2013. ISSN 1873-5118. doi: 10.1016/j.pneurobio.2012.05.013. URL http://www.ncbi.nlm.nih.gov/pubmed/22683381.

M. E. Diamond, M. Armstrong-James, M. J. Budway, and F. F. Ebner. Somatic sensory responses in the rostral sector of the posterior group (POm) and in the ventral posterior medial nucleus (VPM) of the rat thalamus: dependence on the barrel field cortex. *The Journal of comparative neurology*, 319(1):66–84, May 1992. ISSN 0021-9967. doi: 10.1002/cne.903190108. URL http://www.ncbi.nlm.nih.gov/pubmed/1592906.

M. E. Diamond, M. von Heimendahl, P. M. Knutsen, D. Kleinfeld, and E. Ahissar. 'Where' and 'what' in the whisker sensorimotor system. *Nature reviews. Neuroscience*, 9(8):601–12, Aug. 2008. ISSN 1471-0048. doi: 10.1038/nrn2411. URL http://www.ncbi.nlm.nih.gov/pubmed/18641667.

S. Ebara, K. Kumamoto, T. Matsuura, J. E. Mazurkiewicz, and F. L. Rice. Similarities and differences in the innervation of mystacial vibrissal follicle-sinus complexes in the rat and cat: a confocal microscopic study. *The Journal of comparative neurology*, 449(2):103–19, July 2002. ISSN 0021-9967. doi: 10.1002/cne.10277. URL http://www.ncbi.nlm.nih.gov/pubmed/12115682.

R. Emerson, M. Korenberg, and M. Citron. Identification of complex-cell intensive nonlinearities in a cascade model of cat visual cortex. *Biological Cybernetics*, 66(4):291–300, 1992. ISSN 0340-1200. URL http://www.springerlink.com/index/N417H6751T4326RX.pdf.

S. Escola, A. Fontanini, D. Katz, and L. Paninski. Hidden markov models for the stimulus-response relationships of multistate neural systems. *Neural computation*, 23(5):1071–132, May 2011. ISSN 1530-888X. doi: 10.1162/NECO_a_00118. URL http://www.ncbi.nlm.nih.gov/pubmed/21299424.

D. E. Feldman and M. Brecht. Map plasticity in somatosensory cortex. *Science (New York, N.Y.)*, 310(5749):810–5, Nov. 2005. ISSN 1095-9203. doi: 10.1126/science.1115807. URL http://www.ncbi.nlm.nih.gov/pubmed/16272113.

T. Gerdjikov and C. Bergner. Discrimination of vibrotactile stimuli in the rat whisker system: behavior and neurometrics. *Neuron*, 65(4):530–40, Feb. 2010. ISSN 1097-4199. doi: 10.1016/j.neuron.2010.02.007. URL http://www.ncbi.nlm.nih.gov/pubmed/20188657http://www.sciencedirect.com/science/article/pii/S089662731000098X.

J. M. Gibson and W. I. Welker. Quantitative studies of stimulus coding in first-order vibrissa afferents of rats. 1. Receptive field properties and threshold distributions. *Somatosensory research*, 1(1):51–67, 1983. URL http://europepmc.org/abstract/MED/6679913.

E. Guić-Robles, C. Valdivieso, and G. Guajardo. Rats can learn a roughness discrimination using only their vibrissal system. *Behavioural brain research*, 31(3):285–9, Jan. 1989. ISSN 0166-4328. URL http://www.ncbi.nlm.nih.gov/pubmed/2914080.

M. J. Hartmann, N. J. Johnson, R. B. Towal, and C. Assad. Mechanical characteristics of rat vibrissae: resonant frequencies and damping in isolated whiskers and in the awake behaving animal. *The Journal of neuroscience : the official journal of the Society for Neuroscience*, 23(16):6510–9, July 2003. ISSN 1529-2401. URL http://www.ncbi.nlm.nih.gov/pubmed/12878692.

P. Heggelund and K. Albus. Response variability and orientation discrimination of single cells in striate cortex of cat. *Experimental Brain Research*, 32(2):197–211, June 1978. ISSN 0014-4819. doi: 10.1007/BF00239727. URL http://www.springerlink.com/index/10.1007/BF00239727.

J. Hipp, E. Arabzadeh, E. Zorzin, J. Conradt, C. Kayser, M. Diamond, and P. Konig. Texture signals in whisker vibrations. *Journal of neurophysiology*, 95(3):1792–1799, 2006. ISSN 0022-3077. doi: 10.1152/jn.01104.2005. URL http://jn.physiology.org/cgi/content/abstract/95/3/1792.

E. T. Jaynes. *Probability theory: the logic of science*. Cambridge Univ Pr, Cambridge, 2003. ISBN 0 521 59271 2.

L. M. Jones, D. a. Depireux, D. J. Simons, and A. Keller. Robust temporal coding in the trigeminal system. *Science (New York, N.Y.)*, 304(5679):1986–9, June 2004a. ISSN 1095-9203. doi: 10.1126/science.1097779. URL http://www.pubmedcentral.nih.gov/articlerender.fcgi?artid=1557422\&tool=pmcentrez\&rendertype=abstract.

L. M. Jones, S. Lee, J. C. Trageser, D. J. Simons, and A. Keller. Precise temporal responses in whisker trigeminal neurons. *Journal of neurophysiology*, 92(1):665–8, July 2004b. ISSN 0022-3077. doi: 10.1152/jn.00031.2004. URL http://www.pubmedcentral.nih.gov/articlerender.fcgi?artid=2800049\&tool=pmcentrez\&rendertype=abstract.

P. Kara, P. Reinagel, and R. Reid. Low response variability in simultaneously recorded retinal, thalamic, and cortical neurons. *Neuron*, 27(3):635–646, 2000. ISSN 0896-6273. URL http://linkinghub.elsevier.com/retrieve/pii/S0896627300000726.

D. Kleinfeld, E. Ahissar, and M. E. Diamond. Active sensation: insights from the rodent vibrissa sensorimotor system. *Current opinion in neurobiology*, 16(4):435–44, Aug. 2006. ISSN 0959-4388. doi: 10.1016/j.conb.2006.06.009. URL http://www.ncbi.nlm.nih.gov/pubmed/16837190.

D. J. Krupa, M. S. Matell, A. J. Brisben, L. M. Oliveira, and M. A. Nicolelis. Behavioral properties of the trigeminal somatosensory system in rats performing whisker-dependent tactile discriminations. *Journal of Neuroscience*, 21(15):5752–5763, 2001. URL http://www.ncbi.nlm.nih.gov/pubmed/11466447.

J. E. Kulkarni and L. Paninski. Common-input models for multiple neural spike-train data. *Network (Bristol, England)*, 18(4):375–407, Dec. 2007. ISSN 0954-898X. doi: 10.1080/09548980701625173. URL http://www.ncbi.nlm.nih.gov/pubmed/17943613.

P. W. Land and D. J. Simons. Metabolic and structural correlates of the vibrissae representation in the thalamus of the adult rat. *Neuroscience letters*, 60(3):319–24, Oct. 1985. ISSN 0304-3940. URL http://www.ncbi.nlm.nih.gov/pubmed/2999649.

P. W. Land, S. a. Buffer, and J. D. Yaskosky. Barreloids in adult rat thalamus: three-dimensional architecture and relationship to somatosensory cortical barrels. *The Journal of comparative neurology*, 355(4):573–88, May 1995. ISSN 0021-9967. doi: 10.1002/cne.903550407. URL http://www.ncbi.nlm.nih.gov/pubmed/7636032.

Y. Lass and M. Abeles. Transmission of information by the axon. i: Noise and memory in the myelinated fibre of the frog. *Biol Cybern*, 19:61–67, 1975.

B. Lau, G. B. Stanley, and Y. Dan. Computational subunits of visual cortical neurons revealed by artificial neural networks. *Proceedings of the National Academy of Sciences of the United States of America*, 99(13):8974–9, June 2002. ISSN 0027-8424. doi: 10.1073/pnas.122173799. URL http://www.pubmedcentral.nih.gov/articlerender.fcgi?artid=124408\&tool=pmcentrez\&rendertype=abstract.

K. J. Lee and T. a. Woolsey. A proportional relationship between peripheral innervation density and cortical neuron number in the somatosensory system of the mouse. *Brain research*, 99(2): 349–53, Dec. 1975. ISSN 0006-8993. URL http://www.ncbi.nlm.nih.gov/pubmed/1182550.

S. C. Leiser and K. a. Moxon. Relationship between physiological response type (RA and SA) and vibrissal receptive field of neurons within the rat trigeminal ganglion. *Journal of neurophysiology*, 95(5):3129–45, May 2006. ISSN 0022-3077. doi: 10.1152/jn.00157.2005. URL http://www.ncbi.nlm.nih.gov/pubmed/16421201.

S. C. Leiser and K. a. Moxon. Responses of trigeminal ganglion neurons during natural whisking behaviors in the awake rat. *Neuron*, 53(1):117–33, Jan. 2007. ISSN 0896-6273. doi: 10.1016/j.neuron.2006.10.036. URL http://www.ncbi.nlm.nih.gov/pubmed/17196535.

S. Lichtenstein, G. Carvell, and D. Simons. Responses of rat trigeminal ganglion neurons to movements of vibrissae in different directions. *Somatosensory and Motor Research*, 7(1):47–65, 1990. URL http://informahealthcare.com/doi/abs/10.3109/08990229009144697.

E. Lottem and R. Azouz. Dynamic translation of surface coarseness into whisker vibrations. *Journal of neurophysiology*, 100(5):2852–65, Nov. 2008. ISSN 0022-3077. doi: 10.1152/jn.90302.2008. URL http://www.ncbi.nlm.nih.gov/pubmed/18799602.

E. Lottem and R. Azouz. A unifying framework underlying mechanotransduction in the somatosensory system. *The Journal of neuroscience : the official journal of the Society for Neuroscience*, 31(23):8520–32, June 2011. ISSN 1529-2401. doi: 10.1523/JNEUROSCI.6695-10.2011. URL http://www.ncbi.nlm.nih.gov/pubmed/21653856.

B. N. Lundstrom, A. L. Fairhall, and M. Maravall. Multiple timescale encoding of slowly varying whisker stimulus envelope in cortical and thalamic neurons in vivo. *The Journal of neuroscience : the official journal of the Society for Neuroscience*, 30(14):5071–7, Apr. 2010. ISSN 1529-2401. doi: 10.1523/JNEUROSCI.2193-09.2010. URL http://www.ncbi.nlm.nih.gov/pubmed/20371827.

D. MacKay. The limiting information capacity of a neuronal link. *Bulletin of Mathematical Biology*, 14(2):127–135, 1952. ISSN 0092-8240. URL http://www.springerlink.com/index/45123331K651G24X.pdf.

D. MacKay. *Information theory, inference, and learning algorithms*. Cambridge Univ Pr, June 2003. ISBN 0521642981. URL http://books.google.com/books?hl=en\&lr=\&id=AKuMj4PN_EMC\&oi=fnd\&pg=PR11\&dq=Information+Theory,+Inference,+and+Learning+Algorithms\&ots=EJqmf94xGb\&sig=CDwfqFqsof-riOebO0Q8HYlvRo8.

D. J. C. MacKay. Bayesian Interpolation. *Neural Computation*, 4(3):415–447, May 1992. ISSN 0899-7667. doi: 10.1162/neco.1992.4.3.415. URL http://www.mitpressjournals.org/doi/abs/10.1162/neco.1992.4.3.415.

Z. Mainen and T. Sejnowski. Reliability of spike timing in neocortical neurons. *Science*, 1995. URL http://www.sciencemag.org/cgi/content/abstract/sci;268/5216/1503.

M. Maravall, R. S. Petersen, A. L. Fairhall, E. Arabzadeh, and M. E. Diamond. Shifts in coding properties and maintenance of information transmission during adaptation in barrel cortex. *PLoS biology*, 5(2):e19, Feb. 2007. ISSN 1545-7885. doi: 10.1371/journal.pbio.0050019. URL http://www.ncbi.nlm.nih.gov/pubmed/17253902.

P. Z. Marmarelis and V. Z. Marmarelis. *Analysis of physiological systems: The white-noise approach*. Plenum Press, New York, 1978. ISBN 030631066X.

J. Martens and I. Sutskever. Training deep and recurrent networks with hessian-free optimization. *Neural Networks: Tricks of the Trade*, pages 1–58, 2012. URL http://link.springer.com/chapter/10.1007/978-3-642-35289-8_27.

W. S. McCulloch and W. Pitts. A logical calculus of the ideas immanent in nervous activity. *Bulletin of Mathematical Biophysics*, 5(4):115–133, 1943. ISSN 00074985. doi: 10.1007/BF02478259. URL http://www.springerlink.com/index/61446605110620KG.pdf.

M. Miller and K. Mark. A statistical study of cochlear nerve discharge patterns in response to complex speech stimuli. *The Journal of the Acoustical Society of America*, 92(1):202–209, 1992. URL http://link.aip.org/link/?JASMAN/92/202/1.

B. Mitchinson, K. N. Gurney, P. Redgrave, C. Melhuish, A. G. Pipe, M. Pearson, I. Gilhespy, and T. J. Prescott. Empirically inspired simulated electro-mechanical model of the rat mystacial follicle-sinus complex. *Proceedings. Biological sciences / The Royal Society*, 271(1556):2509–16, Dec. 2004. ISSN 0962-8452. doi: 10.1098/rspb.2004.2882. URL http://www.pubmedcentral.nih.gov/articlerender.fcgi?artid=1691889\&tool=pmcentrez\&rendertype=abstract.

B. Mitchinson, E. Arabzadeh, M. E. Diamond, and T. J. Prescott. Spike-timing in primary sensory neurons: a model of somatosensory transduction in the rat. *Biological cybernetics*, 98(3):185–94, Mar. 2008. ISSN 0340-1200. doi: 10.1007/s00422-007-0208-7. URL http://www.ncbi.nlm.nih.gov/pubmed/18180946.

D. Monner and J. a. Reggia. A generalized LSTM-like training algorithm for second-order recurrent neural networks. *Neural networks : the official journal of the International Neural Network Society*, 25(1):70–83, Jan. 2012. ISSN 1879-2782. doi: 10.1016/j.neunet.2011.07.003. URL http://www.pubmedcentral.nih.gov/articlerender.fcgi?artid=3217173\&tool=pmcentrez\&rendertype=abstract.

M. A. Montemurro, S. Panzeri, M. Maravall, A. Alenda, M. R. Bale, M. Brambilla, and R. S. Petersen. Role of precise spike timing in coding of dynamic vibrissa stimuli in somatosensory thalamus. *Journal of neurophysiology*, 98(4):1871–82, Oct. 2007. ISSN 0022-3077. doi: 10.1152/jn.00593.2007. URL http://www.ncbi.nlm.nih.gov/pubmed/17671103.

C. I. Moore and S. B. Nelson. Spatio-temporal subthreshold receptive fields in the vibrissa representation of rat primary somatosensory cortex. *Journal of neurophysiology*, 80(6):2882–92, Dec. 1998. ISSN 0022-3077. URL http://www.ncbi.nlm.nih.gov/pubmed/9862892.

M. a. Neimark, M. L. Andermann, J. J. Hopfield, and C. I. Moore. Vibrissa resonance as a transduction mechanism for tactile encoding. *The Journal of neuroscience : the official journal of the Society for Neuroscience*, 23(16):6499–509, July 2003. ISSN 1529-2401. URL http://www.ncbi.nlm.nih.gov/pubmed/12878691.

J. a. Nelder and R. W. M. Wedderburn. Generalized Linear Models. *Journal of the Royal Statistical Society. Series A (General)*, 135(3):370–384, 1972. ISSN 00359238. doi: 10.2307/2344614. URL http://links.jstor.org/sici?sici=0035-9238(1972)135:3<370:GLM>2.0.CO;2-X\&origin=crossref.

D. H. O'Connor, S. P. Peron, D. Huber, and K. Svoboda. Neural activity in barrel cortex underlying vibrissa-based object localization in mice. *Neuron*, 67(6):1048–61, Sept. 2010. ISSN 1097-4199. doi: 10.1016/j.neuron.2010.08.026. URL http://www.ncbi.nlm.nih.gov/pubmed/20869600.

L. Paninski. Convergence properties of three spike-triggered analysis techniques. *Network (Bristol, England)*, 14(3):437–64, Aug. 2003. ISSN 0954-898X. URL http://www.ncbi.nlm.nih.gov/pubmed/12938766.

L. Paninski. Maximum likelihood estimation of cascade point-process neural encoding models. *Network: Computation in Neural Systems*, 15(4):243–262, Nov. 2004. ISSN 0954-898X. doi: 10.1088/0954-898X/15/4/002. URL http://www.informaworld.com/openurl?genre=article\&doi=10.1088/0954-898X/15/4/002\&magic=crossref||D404A21C5BB053405B1A640AFFD44AE3.

L. Paninski, J. Pillow, and J. Lewi. Statistical models for neural encoding, decoding, and optimal stimulus design. *Progress in brain research*, 165:493–507, Jan. 2007. ISSN 0079-6123. doi: 10.1016/S0079-6123(06)65031-0. URL http://www.ncbi.nlm.nih.gov/pubmed/17925266.

L. Paninski, Y. Ahmadian, D. Ferreira, S. Koyama, K. Rad, M. Vidne, J. Vogelstein, and W. Wu. A new look at state-space models for neural data. *Journal of computational neuroscience*, 29(1-2):107–126, Aug. 2009. ISSN 1573-6873. doi: 10.1007/s10827-009-0179-x. URL http://www.springerlink.com/index/pdf/10.1007/s10827-009-0179-x.

I. Park. Bayesian Spike-Triggered Covariance Analysis. *books.nips.cc*, pages 1–9, 2011. URL http://books.nips.cc/papers/files/nips24/NIPS2011_0954.pdf.

M. Park and J. W. Pillow. Receptive field inference with localized priors. *PLoS computational biology*, 7(10):e1002219, Oct. 2011. ISSN 1553-7358. doi: 10.1371/journal.pcbi.1002219. URL http://www.pubmedcentral.nih.gov/articlerender.fcgi?artid=3203052\&tool=pmcentrez\&rendertype=abstract.

a. Peters and B. R. Payne. Numerical relationships between geniculocortical afferents and pyramidal cell modules in cat primary visual cortex. *Cerebral cortex (New York, N.Y. : 1991)*, 3 (1):69–78, 1993. ISSN 1047-3211. URL http://www.ncbi.nlm.nih.gov/pubmed/8439740.

C. C. H. Petersen. The functional organization of the barrel cortex. *Neuron*, 56(2):339–55, Oct. 2007. ISSN 0896-6273. doi: 10.1016/j.neuron.2007.09.017. URL http://www.ncbi.nlm.nih.gov/pubmed/17964250.

R. S. Petersen, M. Brambilla, M. R. Bale, A. Alenda, S. Panzeri, M. a. Montemurro, and M. Maravall. Diverse and temporally precise kinetic feature selectivity in the VPm thalamic nucleus. *Neuron*, 60(5):890–903, Dec. 2008. ISSN 1097-4199. doi: 10.1016/j.neuron.2008.09.041. URL http://www.ncbi.nlm.nih.gov/pubmed/19081382.

R. S. Petersen, S. Panzeri, and M. Maravall. Neural coding and contextual influences in the whisker system. *Biological cybernetics*, 100(6):427–46, June 2009. ISSN 1432-0770. doi: 10.1007/s00422-008-0290-5. URL http://www.ncbi.nlm.nih.gov/pubmed/19189120.

T. Pierret, P. Lavallée, and M. Deschênes. Parallel streams for the relay of vibrissal information through thalamic barreloids. *The Journal of neuroscience : the official journal of the Society for Neuroscience*, 20(19):7455–62, Oct. 2000. ISSN 1529-2401. URL http://www.ncbi.nlm.nih.gov/pubmed/11007905.

R. Prenger, M. C.-K. Wu, S. V. David, and J. L. Gallant. Nonlinear V1 responses to natural scenes revealed by neural network analysis. *Neural networks : the official journal of the International Neural Network Society*, 17(5-6):663–79, 2004. ISSN 0893-6080. doi: 10.1016/j.neunet.2004.03.008. URL http://www.ncbi.nlm.nih.gov/pubmed/15288891.

R. Quian Quiroga and S. Panzeri. Extracting information from neuronal populations: information theory and decoding approaches. *Nature reviews. Neuroscience*, 10(3):173–85, Mar. 2009. ISSN 1471-0048. doi: 10.1038/nrn2578. URL http://www.ncbi.nlm.nih.gov/pubmed/19229240.

C. Rasmussen and C. Williams. *Gaussian processes for machine learning*. MIT Press, Cambridge, MA, 2006. ISBN 026218253X.

F. Rice, A. Mance, and B. Munger. A comparative light microscopic analysis of the sensory innervation of the mystacial pad. I. Innervation of vibrissal folliclesinus complexes. *The Journal of Comparative Neurology*, 252(2):154–174, Oct. 1986. ISSN 0021-9967. doi: 10.1002/cne.902520203. URL http://www.ncbi.nlm.nih.gov/pubmed/3782505http://onlinelibrary.wiley.com/doi/10.1002/cne.902520203/abstract.

F. L. Rice and B. L. Munger. A comparative light microscopic analysis of the sensory innervation of the mystacial pad. II. The common fur between the vibrissae. *The Journal of comparative neurology*, 252(2):186–205, Oct. 1986. ISSN 0021-9967. doi: 10.1002/cne.902520205. URL http://www.ncbi.nlm.nih.gov/pubmed/3782507.

F. Rieke, D. a. Bodnar, and W. Bialek. Naturalistic stimuli increase the rate and efficiency of information transmission by primary auditory afferents. *Proceedings. Biological sciences / The Royal Society*, 262(1365):259–65, Dec. 1995. ISSN 0962-8452. doi: 10.1098/rspb.1995.0204. URL http://www.ncbi.nlm.nih.gov/pubmed/8587884.

F. Rieke, D. Warland, R. van Steveninck, and W. Bialek. *Spikes: exploring the neural code*. MIT Press, 1999. ISBN 0262181746. URL http://www.amazon.ca/exec/obidos/redirect?tag=citeulike09-20\&\#38;path=ASIN/0262681080http://scholar.google.com/scholar?hl=en\&btnG=Search\&q=intitle:Spikes+:+exploring+the+neural+code\#0.

D. Ringach. Reverse correlation in neurophysiology. *Cognitive Science*, 28:147–166, 2004. doi: 10.1016/j.cogsci.2003.11.003.

J. Ritt and M. Andermann. Embodied information processing: vibrissa mechanics and texture features shape micromotions in actively sensing rats. *Neuron*, 57(4):599–613, Feb. 2008. ISSN 1097-4199. doi: 10.1016/j.neuron.2007.12.024. URL http://www.ncbi.nlm.nih.gov/pubmed/18304488http://www.sciencedirect.com/science/article/pii/S0896627308000275.

F. Rosenblatt. The perceptron: a probabilistic model for information storage and organization in the brain. *Psychological review*, 65(6):386–408, Nov. 1958. ISSN 0033-295X. URL http://www.ncbi.nlm.nih.gov/pubmed/13602029.

D. E. Rumelhart, G. E. Hinton, and R. J. Williams. Learning representations by back-propagating errors. *Nature*, 323(6088):533–536, Oct. 1986. ISSN 0028-0836. doi: 10.1038/323533a0. URL http://books.google.com/books?hl=en\&lr=\&id=FJblV_iOPjIC\&oi=fnd\&pg=PA213\&dq=Learning+representations+by+back-propagating+errors\&ots=zZDj2mGYVQ\&sig=mcyEACaE_ZB4FB4xsoTgXgcbE2ghttp://books.google.com/books?hl=en\&lr=\&id=FJblV_iOPjIC\&oi=fnd\&pg=PA213\&dq=Learning+representations+by+back-propagating+errors\&ots=zZDj2mGYWU\&sig=XiRRKMW637bqaSupPbx01jQp9T8http://www.nature.com/doifinder/10.1038/323533a0.

M. Sahani and J. Linden. How linear are auditory cortical responses? *Advances in Neural Information Processing Systems 15*, 2003.

H. M. Sakai, J. L. Wang, and K. Naka. Contrast gain control in the lower vertebrate retinas. *The Journal of general physiology*, 105(6):815–35, June 1995. ISSN 0022-1295. URL http://www.pubmedcentral.nih.gov/articlerender.fcgi?artid=2216959\&tool=pmcentrez\&rendertype=abstract.

J. Segundo, G. Moore, L. Stensaas, and T. Bullock. Sensitivity of neurones in aplysia to temporal pattern of arriving impulses. *J Exp Biol*, 40:643–667, 1963.

A. Sestokas and S. Lehmkuhle. Response variability of X-and Y-cells in the dorsal lateral geniculate nucleus of the cat. *Journal of neurophysiology*, 59(2):317, Feb. 1988. ISSN 0022-3077. URL http://scholar.google.com/scholar?hl=en\&btnG=Search\&q=intitle:Response+Variability+of+X-+and+Y-Cells+in+the+Dorsal+Lateral+Geniculate+Nucleus+of+the+Cat\#0.

M. N. Shadlen and W. T. Newsome. The variable discharge of cortical neurons: implications for connectivity, computation, and information coding. *The Journal of neuroscience : the official journal of the Society for Neuroscience*, 18(10):3870–96, May 1998. ISSN 0270-6474. URL http://www.ncbi.nlm.nih.gov/pubmed/9570816.

S. M. Sherman. Tonic and burst firing: dual modes of thalamocortical relay. *Trends in neurosciences*, 24(2):122–6, Mar. 2001. ISSN 0166-2236. URL http://www.ncbi.nlm.nih.gov/pubmed/11164943.

M. Shoykhet, D. Doherty, and D. J. Simons. Coding of deflection velocity and amplitude by whisker primary afferent neurons: implications for higher level processing. *Somatosensory & motor research*, 17(2):171–80, Jan. 2000. ISSN 0899-0220. URL http://www.ncbi.nlm.nih.gov/pubmed/10895887.

D. Smyth, B. Willmore, G. E. Baker, I. D. Thompson, and D. J. Tolhurst. The receptive-field organization of simple cells in primary visual cortex of ferrets under natural scene stimulation. *The Journal of neuroscience : the official journal of the Society for Neuroscience*, 23(11):4746–59, June 2003. ISSN 1529-2401. URL http://www.ncbi.nlm.nih.gov/pubmed/12805314.

R. Storchi, M. R. Bale, G. E. M. Biella, and R. S. Petersen. Comparison of latency and rate coding for the direction of whisker deflection in the subcortical somatosensory pathway. *Journal of neurophysiology*, 108(7):1810–21, Oct. 2012. ISSN 1522-1598. doi: 10.1152/jn.00921.2011. URL http://www.ncbi.nlm.nih.gov/pubmed/22815402.

S. Strong, R. Koberle, R. de Ruyter Van Steveninck, and W. Bialek. Entropy and information in neural spike trains. *Physical Review Letters*, 80(1):197–200, 1998. ISSN 1079-7114. URL http://link.aps.org/doi/10.1103/PhysRevLett.80.197.

M. C. Stüttgen, S. Kullmann, and C. Schwarz. Responses of rat trigeminal ganglion neurons to longitudinal whisker stimulation. *Journal of neurophysiology*, 100(4):1879–84, Oct. 2008. ISSN 0022-3077. doi: 10.1152/jn.90511.2008. URL http://www.ncbi.nlm.nih.gov/pubmed/18684907.

V. Talebi and C. L. Baker. Natural versus Synthetic Stimuli for Estimating Receptive Field Models: A Comparison of Predictive Robustness. *The Journal of neuroscience : the official journal of the Society for Neuroscience*, 32(5):1560–76, Feb. 2012. ISSN 1529-2401. doi: 10.1523/JNEUROSCI.4661-12.2012. URL http://www.ncbi.nlm.nih.gov/pubmed/22302799.

M. Teich and S. Khanna. Pulse number distribution for the neural spike train in the cat's auditory nerve. *J Acoust Soc Am*, 77:1110–1128, 1985.

D. Tolhurst, J. Movshon, and A. Dean. The statistical reliability of signals in single neurons in cat and monkey visual cortex. *Vision Res*, 23:775–785, 1983.

W. Truccolo, U. T. Eden, M. R. Fellows, J. P. Donoghue, and E. N. Brown. A point process framework for relating neural spiking activity to spiking history, neural ensemble, and extrinsic covariate effects. *Journal of neurophysiology*, 93(2):1074–89, Feb. 2005. ISSN 0022-3077. doi: 10.1152/jn.00697.2004. URL `http://www.ncbi.nlm.nih.gov/pubmed/15356183`.

H. Van Der Loos. Barreloids in mouse somatosensory thalamus. *Neuroscience letters*, 2(1):1–6, Mar. 1976. ISSN 0304-3940. URL `http://www.ncbi.nlm.nih.gov/pubmed/18181146`.

P. Veinante, M. F. Jacquin, and M. Deschênes. Thalamic projections from the whisker-sensitive regions of the spinal trigeminal complex in the rat. *The Journal of comparative neurology*, 420(2): 233–43, May 2000. ISSN 0021-9967. URL `http://www.ncbi.nlm.nih.gov/pubmed/10753309`.

M. von Heimendahl, P. M. Itskov, E. Arabzadeh, and M. E. Diamond. Neuronal activity in rat barrel cortex underlying texture discrimination. *PLoS biology*, 5(11):e305, Nov. 2007. ISSN 1545-7885. doi: 10.1371/journal.pbio.0050305. URL `http://www.pubmedcentral.nih.gov/articlerender.fcgi?artid=2071938\&tool=pmcentrez\&rendertype=abstract`.

E. Welker and H. Van der Loos. Quantitative correlation between barrel-field size and the sensory innervation of the whiskerpad: a comparative study in six strains of mice bred for different patterns of mystacial vibrissae. *The Journal of neuroscience : the official journal of the Society for Neuroscience*, 6(11):3355–73, Nov. 1986. ISSN 0270-6474. URL `http://www.ncbi.nlm.nih.gov/pubmed/3772437`.

J. Wolfe, D. N. Hill, S. Pahlavan, P. J. Drew, D. Kleinfeld, and D. E. Feldman. Texture coding in the rat whisker system: slip-stick versus differential resonance. *PLoS biology*, 6(8):e215, Aug. 2008. ISSN 1545-7885. doi: 10.1371/journal.pbio.0060215. URL `http://www.ncbi.nlm.nih.gov/pubmed/18752354`.

T. Woolsey and H. Van der Loos. The structural organization of layer IV in the somatosensory region (SI) of mouse cerebral cortex. The description of a cortical field composed of discrete cytoarchitectonic units. *Brain Research*, 17(2):205, 1970. URL `http://www.ncbi.nlm.nih.gov/pubmed/4904874`.

E. Zucker and W. Welker. Coding of somatic sensory input by vibrissae neurons in the rat's trigeminal ganglion. *Brain Research*, 12(1):138–156, 1969. URL `http://linkinghub.elsevier.com/retrieve/pii/0006899369900614`.